Master's thesis

NTNU
Norwegian University of Science and Technology
Faculty of Information Technology and Electrical Engineering
Department of Electric Power Engineering

Siri Kjærstad Wetjen

Investigation of the Transient Recovery Voltage across Circuit Breakers in Networks with Distributed Energy Resources

Master's thesis in Energy and Environmental Engineering
Supervisor: Kaveh Niayesh
June 2019

NTNU
Norwegian University of Science and Technology

Siri Kjærstad Wetjen

Investigation of the Transient Recovery Voltage across Circuit Breakers in Networks with Distributed Energy Resources

Master's thesis in Energy and Environmental Engineering
Supervisor: Kaveh Niayesh
June 2019

Norwegian University of Science and Technology
Faculty of Information Technology and Electrical Engineering
Department of Electric Power Engineering

NTNU
Norwegian University of
Science and Technology

Problem Description

Introduction of renewable power generation methods such as wind and photovoltaic into medium voltage level power distribution systems leads to fundamental changes of the conventional network configurations. Switching devices designed to cope with the stresses, such as transient recovery voltage and short circuit current, in conventional networks are faced to new types of stresses.

In previous investigations, the switching transients in networks with distributed generation have been studied. It has been shown that in some cases much more severe switching transients in such systems may be produced.

In this master thesis, the idea is to investigate the influence of distributed generation units on the stresses applied to circuit breakers. The focus will be on the characteristics of the applied transient recovery voltages.

Preface

This master thesis has been performed as a part of the M.Sc. in Energy and Environmental Engineering. The master thesis was carried out during the spring semester of 2019 in cooperation with the Department of Electric Power Engineering, NTNU, Trondheim. The main object of this report is to investigate the influence of distributed generation units on the stresses applied to switching devices.

First, I would like to thank my supervisor, professor Kaveh Niayesh, for great guidance and feedback during the whole process. I would send a big thank you to Postdoctoral Fellow Ali Kadivar, who has shown great interest in my project and helped me with the simulation models. In addition, I would like to thank Ali Goharrizi from PSCAD support for helping me with solving different numerical issues related to the simulation models. Finally, I would like to thank Assistant Professor Anders Gytri for helping with different technical problems related to the PSCAD-licence and microsoft remote desktop.

Trondheim, June 2019

Siri Kjærstad Wetjen

Abstract

The addition of small scale generating units to the distribution grid comes with many positive aspects. Among these are reduced costs related to re- investments in transmission lines, increased reliability, and an increased share of renewable energy. However, new challenges have occurred due to the new grid configuration and direction of power flow introduced with distributed generation. Among these concerns are the new stresses applied to the circuit breakers, where more severe transient recovery voltages may be produced. On the basis of this, there is a concern that the original breakers located in the distribution grid are operating beyond their limits in the case of distributed generation.

The objective of this thesis has been to investigate how the addition of the distributed energy sources wind power and photovoltaic will affect the transient recovery voltage applied across medium voltage circuit breakers. This was done with the use of two different base case networks created in PSCAD: one wind power network and one photovoltaic network. Since the transient recovery voltage is highly dependent on the network parameters, the effect of changing some of these have been included in this study. This was done with the aim of observing some of the worst case scenarios.

The same short line fault was applied to both the photovoltaic and the wind power network, and the resulting transient recovery voltage was recorded. The resulting transient recovery voltage was then compared to the relevant capability curve for the circuit breaker under investigation. This was done in both the photovoltaic and the wind power network for the same parameter variations. The four parameters that were investigated are: line length, cable length, power flow through the breaker, and the time between the short circuit instant and the contact separation of the circuit breaker.

It was observed that the peak of the transient recovery voltage was kept within the capability of the breaker for all the chosen parameter variations in both the photovoltaic and the wind power network. However, concerning the rate of rise of recovery voltage a great difference between the photovoltaic and the wind network was observed. In the wind power network the rate of rise of recovery voltage exceeded the capability of the breaker for several of the chosen parameter variations. However, in the photovoltaic network the rate of rise of recovery voltage was kept within the breaker limit for all the chosen parameter variations. The explanation to why the steepest rate of rise of recovery voltages observed in this study were seen in the wind power

network could be related to the high fault currents observed in the wind power network compared to the photovoltaic network.

Sammendrag

Tilkoblingen av små-skala kraftproduksjon i distribusjonsnettet har mange positive sider. Dette innebærer blant annet reduserte kostnader relatert til re-investering i transmisjonslinjer, økt pålitelighet, og en økt andel av fornybar energi. Likevel bidrar dette også til nye utfordringer på grunn av endringen i effektflyt og nettkonfigurasjon. Blant disse utfordringene er mer alvorlige transiente gjenopprettelsesspenninger. På bakgrunn av dette er det en bekymring for at kapasiteten til de originale effektbryterne lokalisert i distribusjonsnettet skal overstiges i tilfellet med distribuert kraftproduksjon.

Hensikten med denne masteroppgaven har vært å undersøke hvordan tilkoblingen av distribuerte energikilder påvirker de transiente gjenopprettelsesspenningene som effektbrytere i distribusjonsnettet utsettes for. Dette ble gjort ved hjelp av to ulike sammenlignings nettverk bygd i PSCAD: et vindkraftnettverk og et solkraftnettverk. Siden den transiente gjenopprettelsesspenningen er svært avhengig av parameterne i nettverket, ble også effekten av å endre noen av disse parameterne studert. Formålet med dette var å observere noen av de mest kritiske tilfellene.

Den samme kort-linje feilen ble påtrykt både i solnettverket og i vindnettverket, og den resulterende transiente gjenopprettelsesspenningen ble undersøkt. Den resulterende transiente gjenopprettelsesspenningen ble deretter sammenlignet med den relevante kapasitet-kurven til bryteren. Dette ble gjort i både vindnettverket og solnettverket for de samme parametervariasjonene. De fire parameterne som ble undersøkt er: linjelengde, kabellengde, effektflyt gjennom bryteren, og tiden mellom kortslutning og kontakt-separasjon i bryteren.

Det ble observert at toppverdien til den transiente gjenopprettelsesspenningen var innenfor kapasiteten til bryteren for alle de valgte parametervariasjonene i både vindnettverket og solnettverket. Angående stigningen til den transiente gjenopprettelsesspenningen ble det observert stor forskjell mellom vindnettverket og solnettverket. I vindnettverket ble det observert at stigningen til den transiente gjenopprettelsesspenningen oversteg kapasiteten til bryteren for flere av de valgte parametervariasjonene. På den andre siden, i solnettverket ble det observert at stigningen til den transiente gjenopprettelsesspenningen var innenfor kapasiteten til bryteren for alle de valgte parametervariasjonene. Forklaringen på hvorfor de bratteste stigningene til den transiente gjenopprettelsesspenningen ble observert i vindnettverket kan være relatert til de høye feilstrømmene som ble observert i vindnettverket sammenlignet med solkraftnettverket.

Contents

1 Introduction

The connection of small scale generating units to the distribution grid results in changes in the direction of power flow and the conventional network configuration. In this introduction, an overview is given on; switching operations in distribution networks, generating units used for distributed generation, and how the addition of distributed generation may affect the stresses applied to switching devices. Regarding the generating units, the focus is on photovoltaic and wind power. Concerning the stresses applied to the breakers, the focus is on the transient recovery voltages. The transient recovery voltages will be investigated because it is essential that it is kept lower than the capability of the breaker to have a successful current interruption and thereby a reliable protection of the network.

1.1 Switching in Distribution Networks

The following two paragraphs are described in the project thesis presented in [1], but will be repeated here. When a load is to be connected or disconnected, a planned operation is performed by a load break switch. This breaker type has the ability to break a current in the range of the maximum load current at that specific point in the grid. In addition, the load break switch also has the ability to make a few short-circuit currents and carry this current for one to three seconds [2]. Other planned switching operations are making changes in the network by energizing or de-energizing lines, cables or capacitor banks. All of the mentioned switching functions require interrupting or making currents in the range of the rated load current [2].

In addition to the planned switching operations, there will arise situations where unplanned changes in the network occur such as in the case of a short circuit fault. When a fault happens, the current increases rapidly compared to the normal operation case and has to be cleared as fast as possible. The fault clearing is accomplished by a circuit breaker or a fuse which has the ability to interrupt currents in the range of the typical fault current in the specific location in the grid [2].

1.2 Distributed Generation

The following six paragraphs are described in the project thesis presented in [1], but will be repeated here. According to [3], distributed generation can be defined as: *"generation of electricity located in the distribution grid. The characteristics for distributed generation (also called DG), is that the*

power plants have installed low capacity related to conventional power plants". There are several reasons behind the increase in distributed generation that is seen today. Among these reasons are the increased power quality, grid support such as stabilizing the frequency during a sudden undercapacity, and an increased share of renewable energy [4]. Another positive aspect related to distributed generation is the reduced costs related to re-investments in existing transmission lines [4, 5].

When distributed generation units, such as wind power and photovoltaic power plants, are connected to the main grid as shown in Figure 1, a new grid configuration is obtained. The well known conventional radial power system as shown in Figure 2 with one power source and power flowing only in one way is becoming more like a network system. In a typical conventional grid, the power is generated by large synchronous generators (SGs) placed physically far away from the consumers. A step-up transformer connects the generating unit directly to the transmission system, which transfers the power over long distances to a location closer to the consumers where the voltage is stepped down and distributed through the distribution grid. As opposed to the conventional grid, in a network system with distributed generation, there are two or more generating units connected to the loads, and the power can flow in different directions [6].

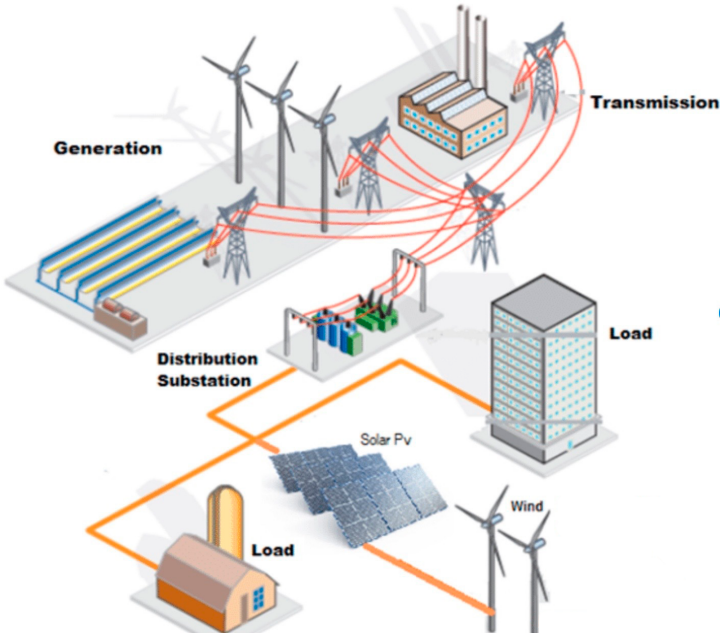

Figure 1: Network with distributed generation, from [7].

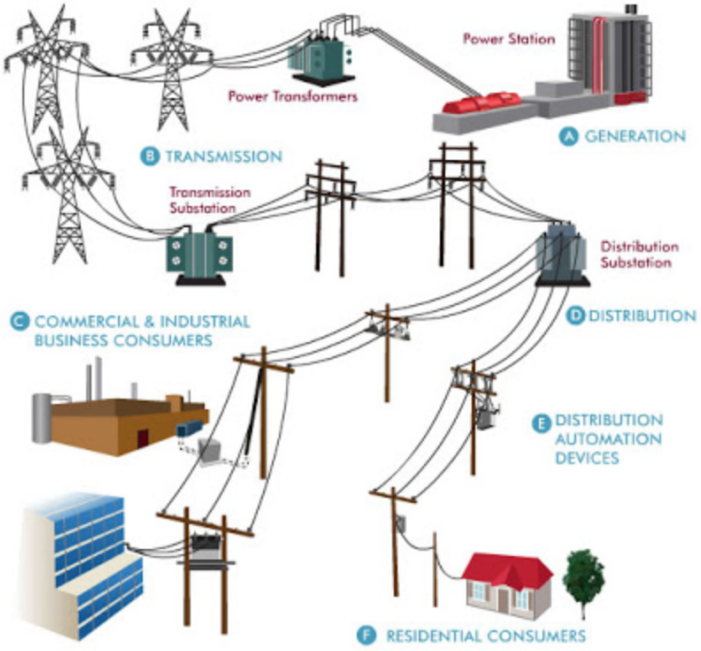

Figure 2: Conventional network configuration, from [8].

1.2.1 Power Generation in Distributed Generation Networks

There is no strict definition that decides whether or not a generating unit can be referred to as distributed generation. According to Pepermans et al. [4], the rated power for a distributed generation unit can be in the range of a few kW to 20 MW. These generating units can be of several different types such as combustion gas turbines, diesel- or natural gas engines, fuel cells, micro turbines, small hydropower generators, wind turbines or photovoltaic systems. In this report, only the renewable energy sources photovoltaic and wind turbines will be discussed. The generated power of both the photovoltaic station and the wind power plant used in this report will be varied in the range of 5-20 MW.

Photovoltaic Generation

This paragraph is based on the theory presented in [9]. A photovoltaic generating unit can have many different configurations. Independent of configuration, the system is always built up by several photovoltaic cells connected in series which form a module. During the design process of a photovoltaic station, it must be decided how many modules should be connected in par-

allel and how many in series to deliver the required power. The combination of several modules forms a photovoltaic array. Further, the PV array is connected to the grid through a DC-DC converter and a DC-AC inverter as shown in Figure 3. Before the output AC current from the inverter is send to the grid, it is passed through an LC or an LCL filter. This filter makes sure that the total harmonic disortion (THD) and the ripple in output voltage and current are kept inside the required limits [10]. Usually, the PV system is equipped with a maximum power point tracker (MPPT) which ensures that the PV modules are operating at the operating point that generates maximum output power. An MPPT is useful as the operating conditions of the PV modules such as temperature [11, 12], irradiation [11, 12], and load [13] will affect the voltage and current generated by the array. Based on the construction of a PV system which differs from a conventional synchronous generator, it is expected to have a different behavior during fault conditions. Consequently, the transient behavior must be thoroughly examined to understand how it would impact the transient recovery voltage.

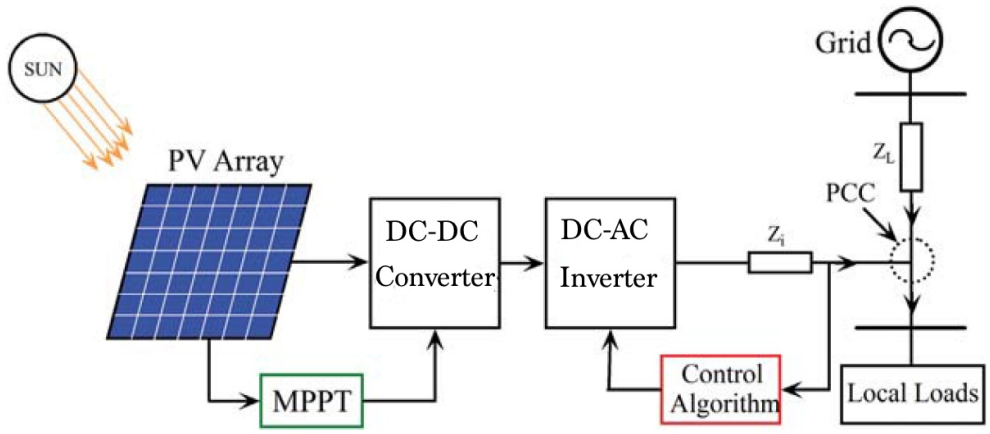

Figure 3: Grid connected photovoltaic system, from [14].

Wind Power Generation

Different configurations of wind power turbines are usually divided into four types [15] depending on the power electronics and the speed control characteristics. The characteristic of a Type 1 turbine is the fixed rotational speed and the direct connection of the stator windings to the grid. As opposed to

Type 1, a generator of Type 2 has a wider operating speed range because of the variable rotor resistance. Both Type 1 and Type 2 are of the induction generator type. A Type 3 generator, also referred to as doubly fed induction generator (DFIG), is a wound rotor induction generator (WRIG) constructed with the rotor connected to the grid through an AC/AC converter and the stator directly connected to the grid as shown in Figure 4. At last, there is the Type 4 generator which is connected to the grid through a full AC/AC converter interface.

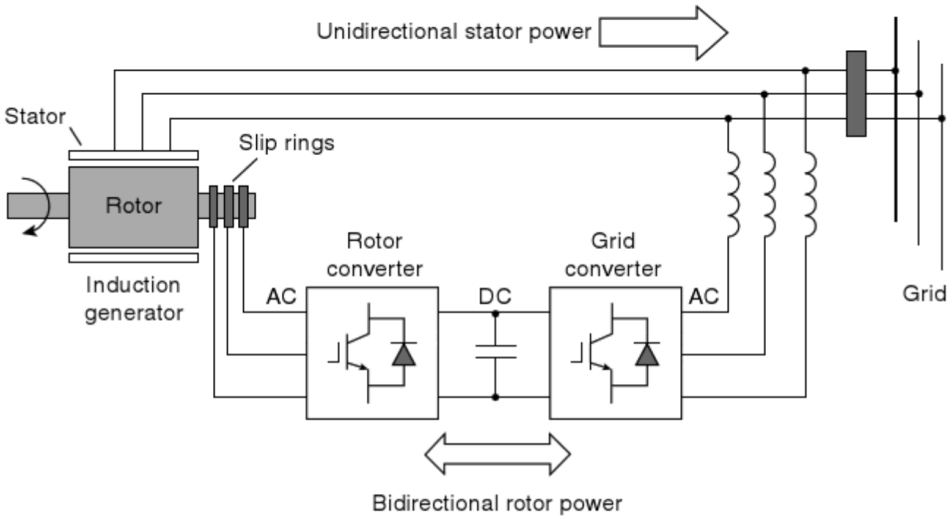

Figure 4: Doubly fed induction generator, from [9].

The DFIG is one of the most popular wind turbine configurations. The reason is that this type can provide good flexibility in rotor speed control and allow control of both reactive and active power flow to the grid from the stator, independent of the speed of the generator [9, 16]. The variable speed is a great advantage as it reduces the mechanical stresses on the turbine drivetrain and the generator [9, 17]. Also, the variable speed is needed for the generator to extract more power from the wind as the wind speed will change. On the basis of this, the DFIG configuration is chosen for the wind turbines discussed in this report. In similarity to the PV system presented above, the DFIG configuration also differs from the conventional synchronous generator, and its transient behaviour should be examined.

1.3 Stresses Applied to Switching Devices

The main parts of the following three paragraphs are described in the project thesis presented in [1], but will be repeated here. The capability of the existing distribution circuit breakers was chosen based on the one-way power flow conventional network shown in Figure 2 [18]. In other words, the circuit breakers in the distribution system were installed with the purpose of protecting networks with loads only, not distributed generation. From this, there is a concern that switching devices are operating beyond their limits in the case of DG [19], due to the new stresses applied to the circuit breakers in this case compared to the conventional network case. In this report, the contribution from distributed generation to the transient recovery voltage will be investigated.

1.3.1 Transient Recovery Voltage

Because the occurrence of a short circuit will result in a higher current flow than at normal conditions, it is important that the fault is cleared as quickly as possible. This is important to avoid damage of equipment such as cables, transformers, and others. It is also important that the fault is cleared within the critical clearing time of the network to avoid stability problems [20]. When a short circuit occurs, the fault is detected and an opening signal is sent to the circuit breaker. The fault is cleared by the current interruption performed by a circuit breaker.

After the current is interrupted at current zero, a voltage referred to as the transient recovery voltage (TRV) is building up across the circuit breaker as shown in Figure 5. The TRV is dependent on the network configuration, the system neutral grounding arrangement, the pre-fault voltage, and the fault current [21]. In some cases, the transient recovery voltage is also dependent on the circuit breaker itself [22]. In addition to the TRV, another voltage referred to as the arc voltage is also shown in Figure 5. The arc voltage is the voltage drop across the arc due to the arcing resistance, which is mainly dependent on the interrupting medium and the design of the switching device [2]. It can be observed that the arc voltage is increasing a bit before current zero. The increased arc voltage before current zero can be explained by noticing that this is the time when the interrupting medium is changing from conducting into insulating. The increased resistance of the arcing medium right before current zero results in a higher voltage drop across the arc at this time instant. However, compared to the transient recovery voltage, the arc voltage is small during the whole arcing period.

Related to the transient recovery voltage, there are two essential parameters used to decide whether the interruption is successful or not: the rate of rise of recovery voltage (RRRV) and the TRV peak. The RRRV can be seen in Figure 6, for the case of a resistive load interruption.

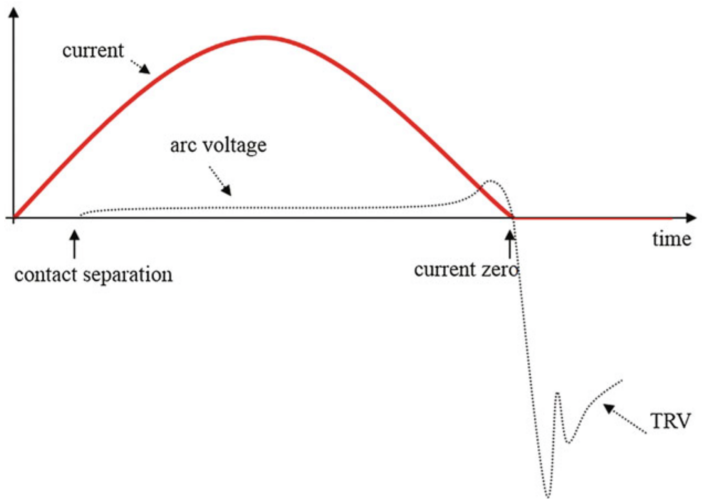

Figure 5: Current and voltage during interruption of short circuit current, from [2].

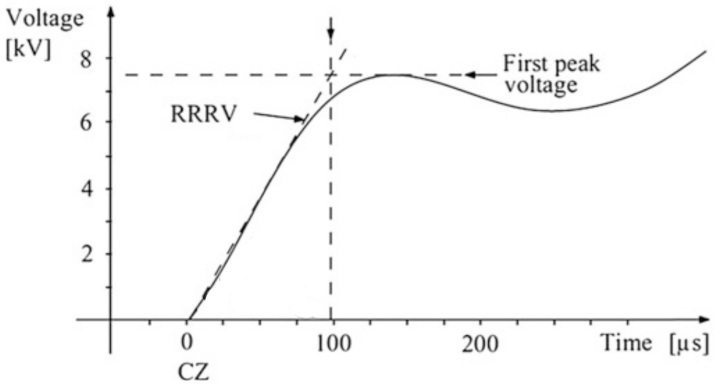

Figure 6: RRRV after breaking a resistive load, from [2].

For the current interruption to be successful it is essential that the transient recovery voltage does not exceed the capability of the circuit breaker at any point. In this thesis, the actual transient recovery voltage will be compared to the relevant capability curves of the breaker under investigation to check

whether or not the capability of the circuit breaker is exceeded. The capability of circuit breakers is defined in standards such as the IEEE-C37.06 [23] and the IEC 62271-100 [24]. The capability curves given in the IEC 62271-100 [24] standard will be used in this report.

1.4 Structure of the Report

The objective of this report has been to:

- Make two base case networks: one base case photovoltaic network and one base case wind power network.
- Use these base case networks to simulate the TRV for different case scenarios of a short line fault. The different case scenarios were used to investigate the effect of changing networks parameters such as: line length, cable length, power flow, and the time between the short circuit instant and the opening operation of the circuit breaker.
- Investigate the simulation results of the different case scenarios to check if the addition of PV and wind power to the distribution grid can lead to a situation where the capability of the breaker is exceeded.

The theoretical background is presented in chapter 2. In this chapter the transient recovery voltage expected in a distribution system is described in detail. In addition, the application of standards, different circuit breaker types and stray capacitance values are discussed in this chapter. Some basic theory related to the chosen wind power configuration and the chosen photovoltaic system are also presented in chapter 2. In chapter 3 the models of both the base case photovoltaic network and the base case wind power network are described. In addition, the special case scenarios used to investigate the effect of changing four network parameters are also presented in chapter 3. The simulation results and a following discussion of these are presented in chapter 4. In addition, some possible source of errors are covered in chapter 4. Finally, the conclusion and suggestions for further work are presented in chapter 5.

2 Theoretical Background

Before the investigation of the TRVs in networks with distributed generation can be performed, some concepts must be understood. The expected fault current should be examined, as the TRVs will depend on this. In addition, some essential theory concerning the transient recovery voltage in networks with distributed generation must be understood. The application of standards, different circuit breaker types and stray capacitances are also covered in this chapter. Finally, some basic concepts regarding the chosen photovoltaic station and the chosen wind power plant are presented.

2.1 Short Circuit Currents in Networks with Distributed Generation

The short circuit current level in a distribution network will increase with the addition of generating units [18, 19, 25]. As opposed to the loads that does not contribute to short circuit current at all, the generating units will contribute to the fault current. In addition to the increased short circuit level, the shape of the fault current might also change as a result of distributed generation.

The fault current contribution from the PV plant and the wind power plant that will be used in this master thesis have been investigated in the project thesis presented in [1]. Even though the networks used in this master thesis are slightly different from the networks used in the project thesis, the general principles of the fault currents are kept. In the project thesis it was observed that the fault current contribution from one PV plant was limited to a peak value of 1 kA due to the control system in the voltage source converter (VSC). In addition, there was not observed any DC component in the fault current contribution from the PV station.

As opposed to the PV case, the fault current contribution from the wind power plant resulted in a high DC component. The explanation behind this DC component is the time dependent inductance that occurs as a result of a fault near the terminal of the wind power plant. This DC component results in a missed current zero for some short circuit instants. In addition, higher amplitudes of the short circuit current can be observed in cases with large DC components [2].

2.1.1 Interruption of Short Circuit Currents

The following paragraph is described in the project thesis presented in [1], but will be repeated here. When a short circuit fault is detected, an opening signal is sent to the circuit breaker. The separation of the switching contacts will start when this signal is received, independent of the value of the current at the time of separation. The contact separation results in ignition of an electrical arc. The interruption of the current can only occur at the zero crossings because there is no energy input into the arc at current zero. Usually, it takes a few microseconds after the zero crossing before the current flow is interrupted [21, 22]. The arcing time (time from arc initiation until arc extinction) will depend on the value of the current at the time of contact separation. Normally, the current will have zero crossings for each half cycles, and typical arcing times are in the range of 0.5-1.5 half cycles, i.e. 5-15 ms in a 50 Hz system [2].

2.2 Transient Recovery Voltage in Networks with Distributed Generation

The next seven paragraphs are described in the project thesis presented in [1], but will be repeated here. When the arc extinguishes, the transient recovery voltage builds up across the circuit breaker. As mentioned earlier, there are two parameters regarding the TRV that must be investigated to check whether a current interruption is successful or not, which is the RRRV and the peak of the TRV. The RRRV is highly dependent on the frequency of the TRV, and higher the frequency is the steeper the RRRV could become [2, 26]. If the RRRV is high, the current can start to flow again in the first few microseconds after current zero; a *thermal re-ignition* occurs. On the other hand, if the breaker interrupts the current for these first microseconds, but the current starts to flow again, it is referred to as a *dielectric re-ignition*. Both the rate of rise of recovery voltage and the peak transient recovery voltage will depend on the shape of the TRV and the system grounding.

2.2.1 Shape of Transient Recovery Voltage

The shape of the transient recovery voltage will depend on several parameters, such as the connected distributed and lumped capacitive and inductive parameters [22, 27] and the location of the fault. The different shapes of the TRVs that can occur in a distribution network can be divided into:

1. Oscillatory

2. Saw-tooth like

3. Overdamped

The oscillatory TRV may occur, for instance, in the case where a fault is located near one of the breaker terminals of a circuit breaker used to protect a transformer [2]. The oscillatory shape can be seen in Figure 7, and it is the result of energy exchange between lumped inductive and capacitive elements in the circuit. The frequency of these oscillations is typically in the range of a few hundred hertz to a few kilohertz [2].

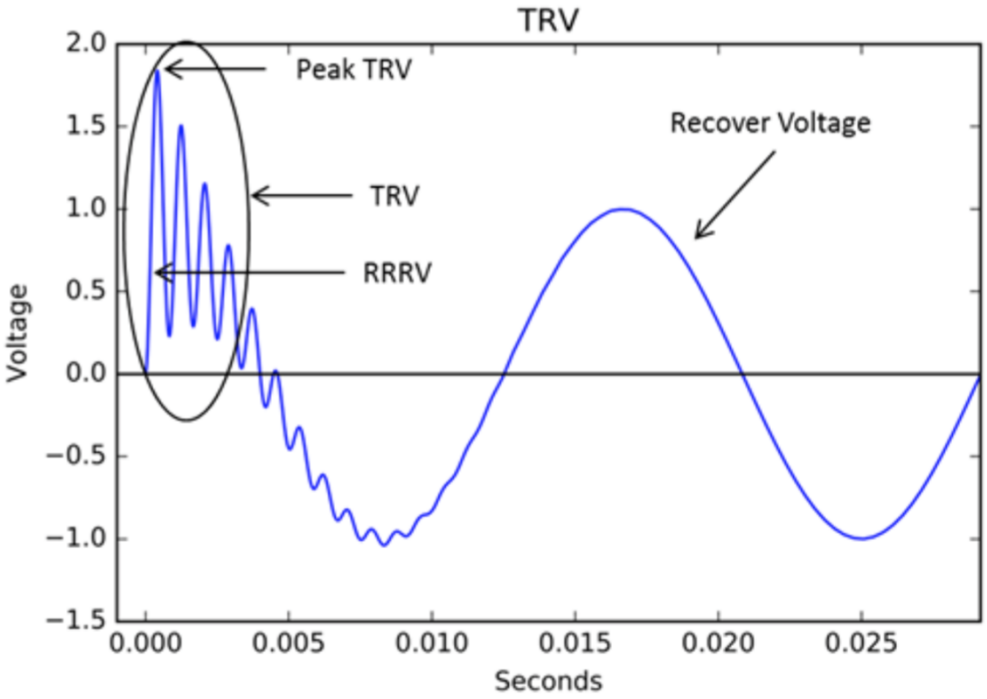

Figure 7: Oscillatory shaped TRV and the remaining voltage when the TRV is damped out referred to as Recovery Voltage, from [28].

If the fault does not occur at the breaker terminal, but at some distance away from the switchgear, the resulting TRV can have a saw-tooth like shape as shown in Figure 8. In this case, the TRV might consist of two high frequency components in addition to the power frequency component [2]. One part with a frequency in the range of a few hundred kilohertz due to the traveling waves on the short line between the fault location and the breaker. A second part with a frequency of a few kilohertz due to the inductance and capacitance from the other side of the breaker.

For this saw-tooth shaped TRV, the rate of rise of recovery voltage usually is the critical parameter that decides whether the current interruption is successful or not [2]. Among other parameters, the RRRV in this case depends on the wave impedance of the line/cable between the switchgear and the fault location. The wave impedance of a line is typically in the range of 300-500 Ω, while the wave impedance of a power cable is typically in the range of a few tens Ω [29, 30]. A higher wave impedance leads to a higher RRRV, which means that the interruption of a short line fault in an overhead line generally is more critical than the case of a short line fault located in a power cable [2]. A fault is referred to as a short line fault if it occurs at a distance of a few hundred meters to a few kilometers away from the breaker [2, 30, 31]. Usually, only high voltage breakers are tested for short-line faults. However, due to the new network configuration introduced with distributed generation it could be expected different TRVs resulting from a short-line fault in a network with DG compared to a conventional distribution network. Based on this, the resulting TRV from a short line fault will be investigated in this report, thus the saw-tooth shape is expected.

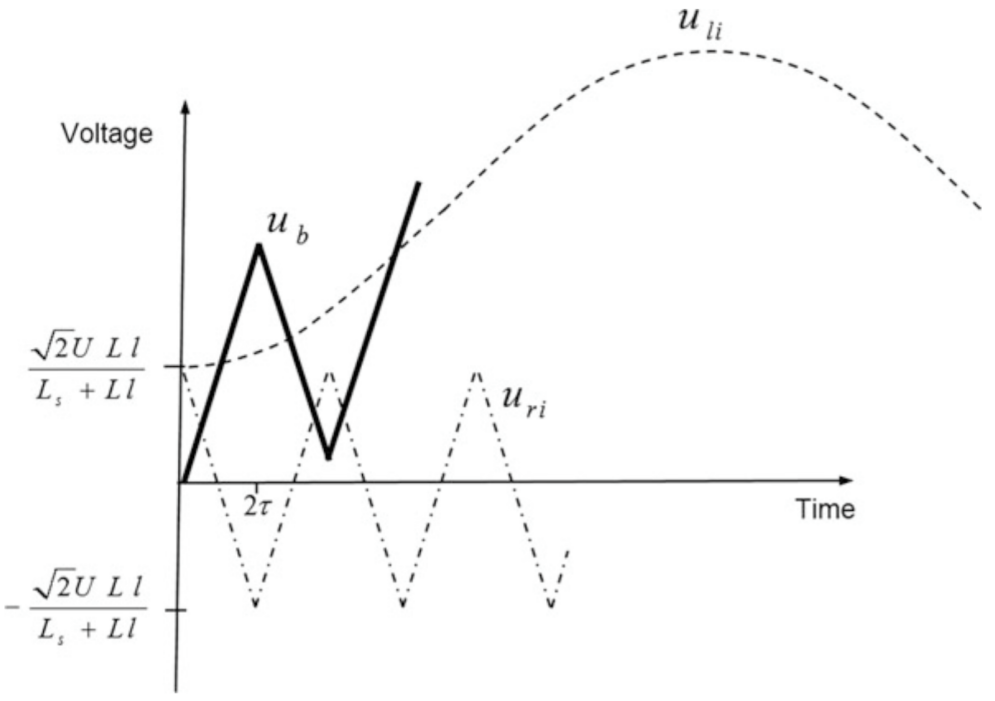

Figure 8: Saw-tooth like TRV, from [2].

In addition to the oscillatory and saw-tooth shape of the TRV, the over-

damped voltage pulse is also a possible TRV shape. The overdamped TRV might be observed in the case where a fault occurs near a breaker connected to a bus bar with many interconnected overhead transmission lines [2]. As the scope of this report is limited to the distribution network, this shape of TRV is excluded from this report.

2.2.2 Grounding Impact on TRV

Usually, in three phase medium voltage networks, the three circuit breakers of each phase are opening at the same time [26], and the current waveform will decide which of the three phases that clears the fault first. The phase where the current is first interrupted is referred to as *first pole or first phase to clear*. In a situation where the network neutral is isolated from ground (or grounded through a high impedance), the current interruption can become more difficult in the first phase compared to the two last phases. This phenomenon is caused by a potential shift of the neutral point [2]. The most severe transient recovery voltages from the amplitude point of view are usually observed in the case of three-phase ungrounded faults [27, 28].

2.3 Application of Standards

As mentioned earlier, the IEC 62271 - 100 [24] standard is used in this thesis to obtain the relevant capability curves. Before the capability curves can be obtained, the following factors must be decided:

- Breaker rated voltage U_r
- Cable system S1 or line system S2
- First pole to clear factor K_{pp}

In the IEC 62271 - 100 [24] the circuit breakers are divided in two categories dependent on the rated voltage: above 100 kV or below 100 kV. The rated voltage U_r is defined in IEC 62271 - 1 [32] as: *"the phase-to-phase RMS voltage equal to the maximum voltage for which the equipment is designed"*. The choice of U_r value used in this report is based on the rated line-to-line RMS voltage in the networks under investigation which is 22 kV. In addition, it is assumed a margin of 7 %, which results in a proper rated maximum voltage of 23.54 kV. By comparing this rated maximum voltage of 23.54 kV to the set of U_r values given in the standard [24], the $U_r = 24$ kV is chosen.

Since this thesis is focusing on the distribution voltage level, which corresponds to rated voltages in the range of 6-36 kV [2], the breaker class of

100 kV and below is used. For circuit breakers rated 100 kV and below, the standard classifies the breakers into two classes, i.e., S1 and S2 [24]. Circuit breakers of class S1 are used in a cable system, while circuit breakers of class S2 are used in a line system. In the studies performed in this thesis, both of these breaker classes (S1 and S2) will be used, as there will be performed simulations on a cable system and on a line system.

The third factor that must be decided before the capability curves can be obtained is the first pole to clear factor K_{pp}. The first pole to clear factor is a result of the different zero crossing times of the current flowing through different poles in a three phase system. This factor depends on the grounding of the system. The standard value used in systems with ungrounded neutral is $K_{pp} = 1.5$, while the standard value used in effectively grounded systems is $K_{pp} = 1.3$ [22]. All the components in the network should be solidly grounded for the $K_{pp} = 1.3$ to be used. In the networks used in this thesis, the sources and the transformers are solidly grounded, but not the overhead lines, underground cables and the induction machine used in the wind power network. Consequently, the $K_{pp} = 1.5$ is used in all the simulations performed in this report.

When the breaker rated voltage, the first pole to clear factor, and the type of system (cable or line) are decided, the corresponding capability curves can be found in the IEC 62271 - 100 [24]. For breakers with rated voltages lower than 100 kV a two-parameter representation of the capability curves is used.

The two-parameter TRV representation consists of a set of U_c and t_3 parameters, where U_c is the TRV peak value given in kV, and t_3 is the time it takes to reach U_c in μs. The general principle of the two-parameter transient recovery voltage representation is shown in Figure 9.

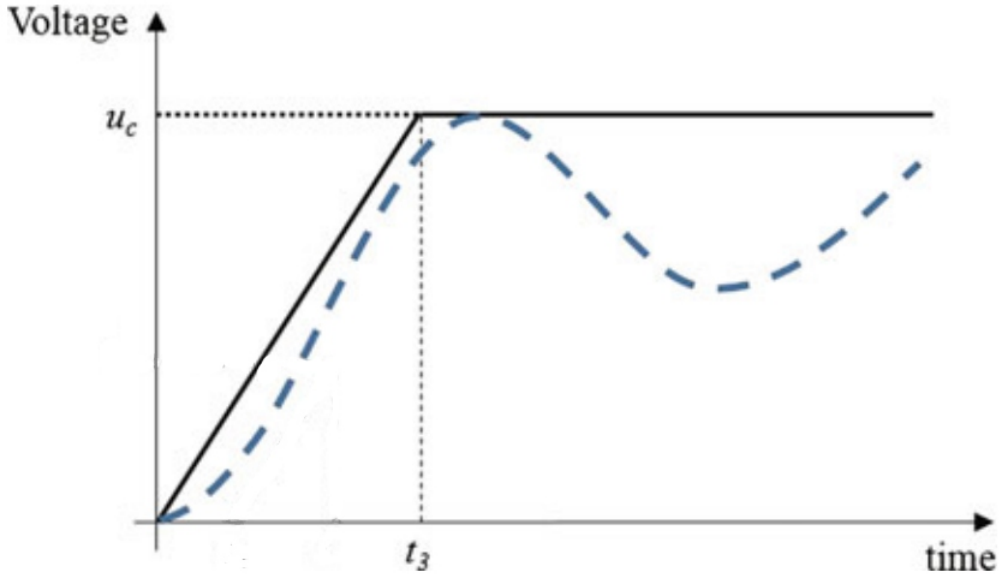

Figure 9: Two-parameter TRV representation, from [2].

Table 1: Two-parameter TRV representation for class S1 circuit breakers for $K_{pp} = 1.5$ and $U_r = 24$ kV, from [24].

Test duty [-]	**TRV peak value U_c** [kV]	**Time t_3** [μs]	**Rate of Rise RRRV** [kV/μs]
T100	41	87	0.47
T60	44.1	38	1.16
T30	47.0	19	2.47
T10	50	19	2.63

Table 2: Two-parameter TRV representation for class S2 circuit breakers for $K_{pp} = 1.5$ and $U_r = 24$ kV, from [24].

Test duty [-]	**TRV peak value U_c** [kV]	**Time t_3** [μs]	**Rate of Rise RRRV** [kV/μs]
T100	45.3	43	1.05
T60	48.4	29	1.67
T30	51.2	17	3.01
T10	52.9	17	3.11

Table 1 and Table 2 summarizes the two-parameter values used in this report

for four different test duties. Table 1 is used for the simulations in a cable system (class S1) while Table 2 is used for simulations in a line system (class S2). All the values in both of the tables are valid for $K_{pp} = 1.5$ and $U_r =$ 24 kV. The different test duties (T10-T100) correspond to the percentage of interrupting rating. If the actual short circuit current is between 60-100 % of the rated breaking capacity, the T100 curve should be used. If the actual short circuit current is between 30-60 % of the rated breaking capacity the T60 capability curves should be used, and so on. The rated breaking capacity is defined in [33] as: *"A value of prospective current that a switching device or a fuse is capable of braking at a stated voltage under prescribed conditions of use and behavior"*. Consequently, which of the four different test duties that should be used in this report depends on the rated breaking capacity of the circuit breaker under investigation, and the actual short circuit current in the network.

2.4 Circuit Breaker Types

As mentioned earlier, the rated voltage of the circuit breaker (U_r) used in this thesis is set to 24 kV. In addition to the rated voltage, the rated current of the circuit breaker must be decided. With the use of steady state simulations of the networks under investigation, it was observed that the nominal current through the circuit breaker under investigation did not exceed a peak value of 1 kA. This observation is valid for both the wind network and the PV network, with a generated power in the range of 5-20 MW. By comparing this peak current to circuit breakers on the market with a rated voltage of 24 kV a rated current of 1250 A was decided.

Table 3: Different Circuit Breakers from ABB with a rated voltage U_r = 24 kV and a rated current of 1250 A, from [34–36].

Name	**Breaker Type**	**Mechanical Operation**	**Rated Breaking Capacity [kA]**	**Opening Time [ms]**	**Arcing Time [ms]**
VD4	Vacuum	Spring-Operated Mechanical Actuator	25	33-60	10-15
VM1	Vacuum	Magnetic Actuator	25	35-50	10-15
HD4	SF_6	Spring-Operated Mechanical Actuator	25	35-60	10-15

Medium voltage circuit breakers of both the vacuum type and the gas type are produced by different manufacturers. In this study, some of the medium voltage breakers provided by ABB are considered, which are presented in Table 3. The table shows the name of the breaker, breaker type, mechanical operation, rated breaking capacity, opening time and arcing time. The opening time of a circuit breaker is defined in [37] as follows: *"the interval of time between the specified instant of initiation of the opening operation and the instant when the arcing contacts have separated. The opening time includes the operating time of any auxiliary equipment necessary to open the circuit breaker"*. The opening time will among other things depend on the breaker configuration and the operating temperature.

In Table 3 it can be observed that all the three breaker types have a rated breaking capacity of 25 kA. Both the VD4 [34] and VM1 [35] are vacuum breakers, but they have different mechanical operation mechanisms. The VD4 breaker has a spring-operated mechanical actuator while the VM1 breaker has a magnetic actuator. The opening time is dependent on the mechanical operation, and the difference in mechanical operation between VD1 and VM1 is probably one of the reasons behind the difference in operating time. In similarity to the VD4, the HD4 [36] SF_6 circuit breaker does also use a spring-operated mechanical actuator. However, there is a slight difference in operating time between the VD4 and the HD4 circuit breaker despite the similarity in operating mechanism.

2.5 Stray Capacitances

In the simulations performed in the project thesis presented in [1] it was observed that the stray capacitance had a great impact on the transient recovery voltage. In addition, the importance of including stray capacitances is mentioned in several TRV studies [21, 26, 27]. Based on this, all the values of stray capacitance used in this thesis are obtained from the IEEE Standard C37.011 [22]. In this standard, the stray capacitance of the current transformer, potential transformer, and the transformer bushing are given as a range of values that are valid for rated voltages in the range of 15-72.5 kV. Inside this range, the stray capacitance of a component is assumed to decrease with an increasing voltage level due to the increased insulation used for higher voltage levels. This phenomenon was accounted for during the selection of the stray capacitances of these components. A summary of the chosen stray capacitances are presented in Table 4.

Table 4: Stray capacitances used in the networks used to simulate TRVs, from [22].

Component	**Stray capacitance [pF]**
Circuit breaker (closed)	50
Circuit breaker (open)	50
Disconnector switch (closed)	100
Air insulated busbar (30m)	1500
Current transformer	200
Potential transformer	400
Lightening arrester	120
Transformer	500

The stray capacitance of the circuit breaker is dependent on whether the breaker is open or closed. Based on this, a stray capacitance of 50 pF was used on each side of the circuit breakers. In this way, the resulting capacitance will be 50 pF if the breaker is open, and 100 pF if the breaker is closed. The stray capacitance used for the circuit breaker is valid for circuit breakers of both the vacuum and the SF_6 type. The stray capacitance of the disconnector switch is valid for the outdoor type.

Concerning the stray capacitance of the busbar, it is assumed that the busbar is air insulated and has a length of 30 m. It is assumed a stray capacitance of 50 pF/m, which results in: 50 pF/m * 30 m = 1500 pF.

Concerning the inductive instrument transformers referred to as current transformer and potential transformer, the stray capacitance was set to 200 pF and 400 pF, respectively. The capacitance of the transformer bushing was set to 500 pF.

2.6 Photovoltaic System Theory

The following two paragraphs are described in the project thesis presented in [1], but will be included here. As mentioned earlier, a photovoltaic generation unit consists of many PV cells, which form a PV array. The equivalent circuit of these cells is shown in Figure 10. The current generated due to the solar irradiation is represented by an ideal DC current source named I_{sc}. I_d is the current through the diode, I_{sh} is the current through a shunt resistance, while I is the output current from one cell. Dependent on how these cells are connected a total DC output voltage and a total DC current is generated, which will be the total output from the PV array.

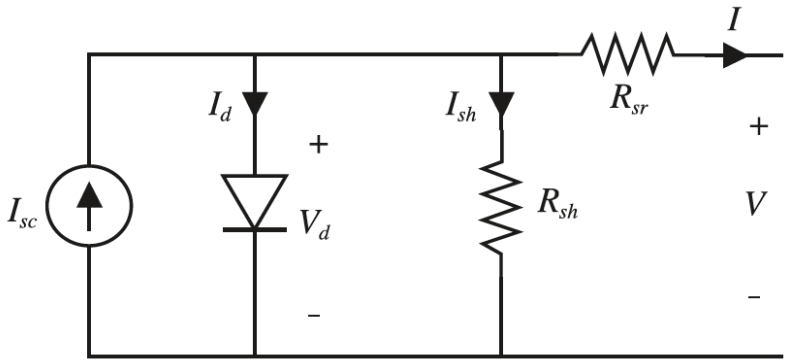

Figure 10: Equivalent circuit of a PV cell, from [13].

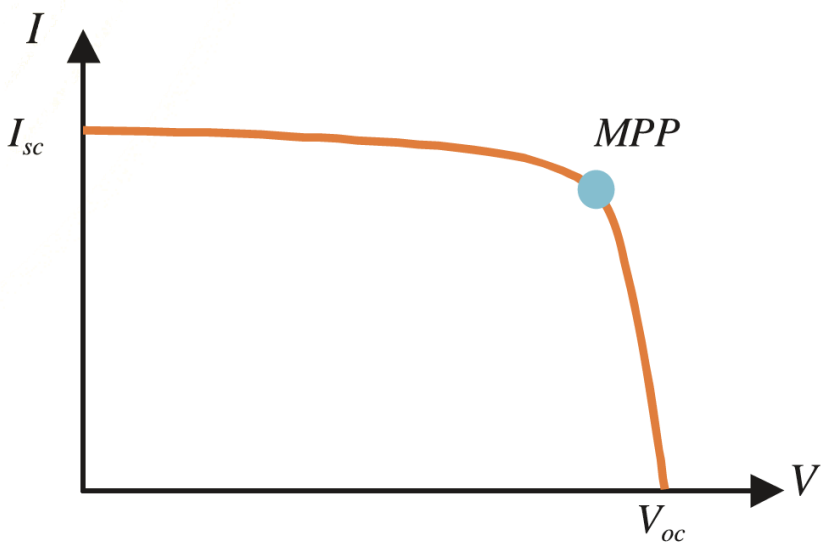

Figure 11: Typical I-V characteristics of a PV cell, from [13].

The I_{sc} from Figure 10 can be recognized in Figure 11, where a typical I-V characteristic of a PV cell is shown. The MPP is the maximum power point, which is the operating point where the PV cell is generating maximum power. The shape of this curve depends on the ambient temperature, solar irradiance, and shading of the cells [9]. From Figure 11 it can be observed that the highest current output from one PV cell is the I_{sc} value. The total I_{sc} and V_{oc} from the PV array depends on the number of cells connected in series and in parallel. Based on this total I-V curve, the power rating and current limits of the inverter used to connect the PV array to the grid are chosen. For the PV model used in the simulations performed in this thesis, the PV array is modeled as a DC voltage source.

2.7 Wind Power System Theory

The following paragraph is described in the project thesis presented in [1], but will be repeated here. The theory covered in this section is based on the dissertation performed by Howard presented in [15]. As mentioned earlier, the chosen type of wind turbine generator in this project is a doubly fed induction generator (Type 3). A construction scheme of the chosen generator type can be seen in Figure 12, and it can be observed that the rotor side converter (RSC) is connected to the rotor, while the grid side converter (GSC) is connected to the stator terminal. Between the RSC and the GSC a DC chopper is placed and the task of this component is to protect the DC link

capacitor (v_{dc}) from high voltages. To protect the rotor-side converter from overcurrents, an AC crowbar is located between the rotor and the RSC.

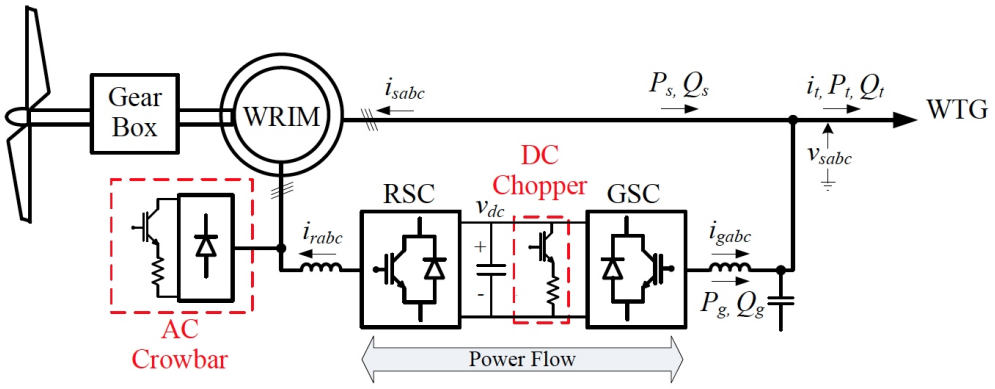

Figure 12: The construction of a doubly fed induction generator, from [15].

3 Modeling

In this thesis there have been made two different base case networks that were used to perform the simulations. One base case photovoltaic network and one base case wind power network. After some general modeling aspects have been discussed, both of the base case networks will be presented, and a detailed explanation of the network components will be given. To examine the worst TRV condition, the effect of changing four different network parameters will be investigated with the use of special case scenarios. These special case scenarios will be described at the end of this modeling chapter.

3.1 General Modeling Aspects

This paragraph is taken from the project thesis presented in [1]. The modeling was performed in PSCAD/EMTDC. PSCAD is a Power Systems Computer Aided Design which uses an electromagnetic transient simulation engine called EMTDC. The PSCAD simulation tool enables the user to build different circuit configurations, run simulations and analyze the results with the use of plotting functions, meters, and controls [38]. In addition to a well-equipped master library of components, PSCAD also has a website with a knowledge base [39] where models that can be used for engineering applications are provided. In this study, two of the provided models from the PSCAD knowledge base were used: the *Grid-connected Photovoltaic System* and the *Type 3 Wind Turbine Generator*.

3.1.1 Fault Model

The fault type used in all the simulations performed in this thesis is a three-line ungrounded fault. This fault type was chosen because the most severe transient recovery voltages from an amplitude point of view are usually observed in the case of three-line ungrounded faults [27, 28]. The fault resistance is set to 50 mΩ, and the fault duration is 400 ms. Typical fault resistances in the range from 1-50 mΩ was tried, and it was observed that changing the fault resistance did not affect the simulation results. The fault duration was set to 400 ms to make sure that the transients occurring when the fault duration is over, do not affect the TRV that arises due to the current interruption in the circuit breaker.

3.1.2 Plotting of the Capability Curves and the Transient Recovery Voltage

The TRV simulation results were obtained by plotting the instantaneous output of a voltmeter connected across the terminals of the circuit breaker under investigation. PSCAD suggests that the time step should be smaller than 1/10 of the shortest wave travelling time in the system. The wave travelling time of each line/cable is calculated by PSCAD at the beginning of each simulation run and can be found in an output file. The shortest wave travelling time will depend on the length of the shortest line/cable in the network, which is 600 m. As the same length is used for cables and lines in this study, the wave travelling time for the shortest line will result in the smallest time step since the wave speed in cables is lower than the wave speed in lines [29]. For a wave speed of $3 * 10^8$ m/s, this results in a wave travelling time of:

$$\tau = \frac{600m}{3 * 10^8 m/s} = 2\mu s.$$

Due to the recommendation from PSCAD, a time step of 0.19 μs was chosen to obtain a sufficient resolution in the output. This time step was used in all the simulations performed in this study, and it is within the range of typical time steps used for TRV simulations performed in PSCAD [27, 40].

The relevant capability curves for the circuit breaker under investigation were plotted with the use of the *TRV Envelope Component* provided by an intermediate library in PSCAD. This component makes sure that the capability curves are plotted exactly at the point on the time axis where the current in the chosen circuit breaker is interrupted and the TRV arises. The capability curves for the relevant test duty presented in Section 2.3 were plotted in the same graph as the TRV for each of the three phases. This was done to compare the actual TRV to the relevant capability curves, and thereby check if the TRV exceeded the capability curves at any point. In addition to a visual inspection, the comparison between the TRV and the relevant capability curve is also done by the *TRV Envelope Component*, and the user is informed with the exact time instant of the violation.

3.2 Base Case Networks

In a TRV study of switching devices it is important that a sufficient part of the network is included. Sufficient in this case is referred to a model of the network system 1-2 buses away from the switching device under investigation [28]. In addition, it is important to ensure that the maximum possible short

circuit current is used in the current interruption study [28]. Both of these aspects were considered when the base case networks were made. In the following sections, the base case photovoltaic network and the base case wind power network are presented.

3.2.1 Base Case Photovoltaic Network

The model of the photovoltaic plant used in this thesis is shown in Figure 13. This PV system deviates from the *Grid-connected Photovoltaic System* [39] provided from PSCAD in one way. The original PV array from the provided PV model in PSCAD was replaced by a DC voltage source. In this way, the original output voltage from the PV array (V_{pv}) of 0.63 kV was kept. This replacement was necessary since the original PV array was not numerically stable for very small time steps. The replacement of the PV array will not affect the behavior of the PV system in this study since the dynamics of the PV array are much slower compared to the TRV transients.

By inspecting Figure 13 it can be observed that a DC voltage (V_{pv}) and a DC current (I_{pv}) is generated at the output of the DC voltage source. Then, the DC current flows through a DC-DC boost converter. The DC-DC boost converter passes out the voltage source converter (VSC) set-voltage (*VDC2*) and a DC current referred to as I_{pvHV}. The VSC receives I_{pvHV} and *VDC2* and converts these DC quantities into AC quantities. The AC-side of the VSC is then further connected to the network. The LCL-filter connected between the VSC terminal and the grid is not shown in Figure 13, as this is placed inside the VSC-component. The LCL-filter is shown in Figure 14.

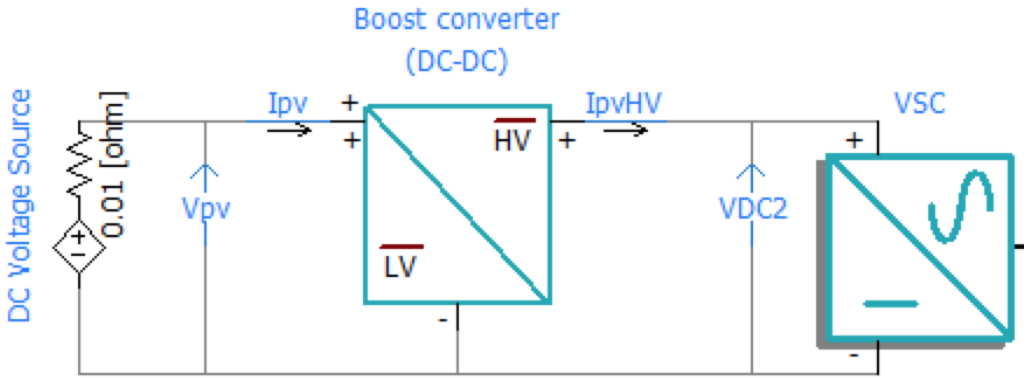

Figure 13: PV power plant model. The photovoltaic system can be connected to a grid by adding a connection to the right side of the VSC.

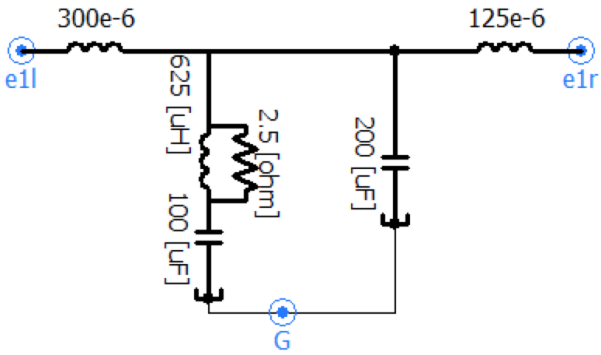

Figure 14: The LCL-filter placed inside the VSC component.

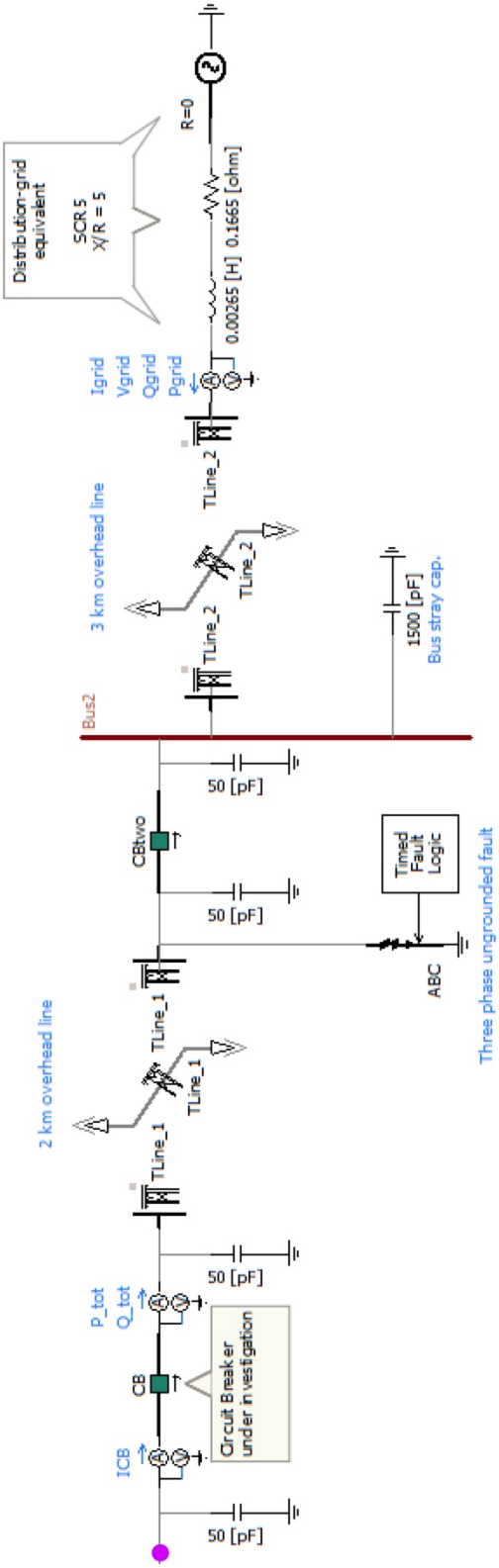

Figure 15: Part 1 of the total network used to simulate TRVs in the grid-connected photovoltaic system.

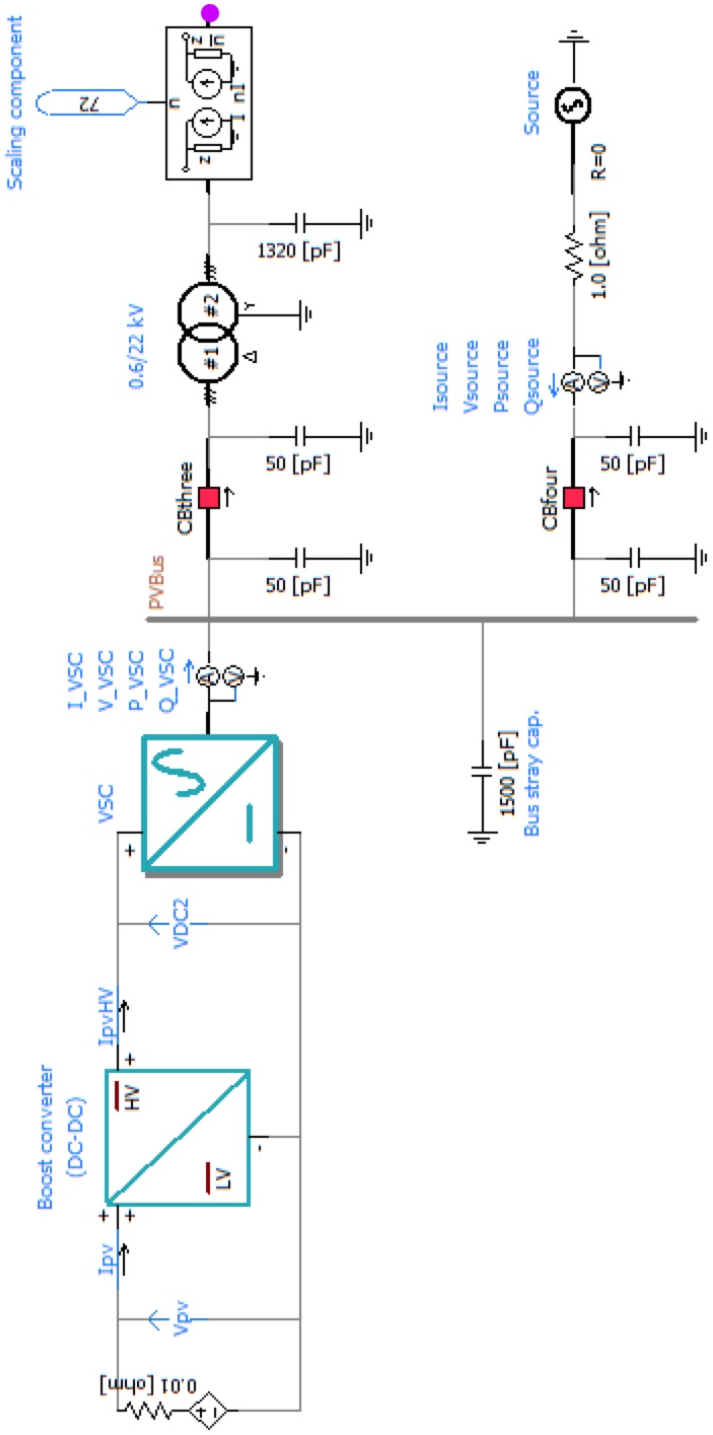

Figure 16: Part 2 of the total network used to simulate TRVs in the grid-connected photovoltaic system.

In Figure 15 and Figure 16 part 1 and part 2 of the total base case photovoltaic network are presented, respectively. The two parts are in reality connected at the pink dots. The steady state values of all the parameters listed above the multimeters can be found in Appendix I.

In this network, the photovoltaic station is connected to the distribution grid through one line of 2 km named *TLine_1* and one line of 3 km named *TLine_2*. The circuit breaker under investigation is named *CB*. When the fault occurs, it is assumed that *CB* is opening first, while the breaker named *CBtwo* is opening 200 ms after *CB* opens. This is because *CBtwo* has to wait 200 ms to check if the fault was cleared by *CB* or not. In the base case PV network the circuit breaker named *CB* are opening 43 ms after the short circuit occurred.

At the bus named *PVBus*, there is also a source connected through a resistance of 1 Ω. This source had to be used in the PV network to make sure that the PLL in the DC-AC converter has a reference when the PV plant is disconnected from the rest of the network (when *CB* is open). The resistance between the source and the *PVbus* was chosen as high as possible while avoiding resonance phenomena to reduce the contribution from this source during short circuit. This source is connected to the rest of the network at all times (*CBfour* is always in closed state). Since some power will be consumed by the source, and the scaling component only works with integers, it was not possible to get exactly 20 MW of active power flowing through the breaker under investigation. A scaling number of 72 resulted in 19.89 MW of power flowing through the circuit breaker under investigation, which is rounded up to 20 MW in the rest of the report.

All the stray capacitance values used in this network are presented in Table 4 in Section 2.5. The 1320 pF stray capacitance placed at the terminal of the 0.6/22 kV transformer is the sum of the stray capacitance of a potential transformer, current transformer, lightening arrester, disconnector switch and the transformer bushing.

Table 5: Photovoltaic System Parameters

Parameter	Value
System Frequency	50 Hz
System Voltage	22 kV L-L, RMS
Rated Output Power from one PV Array	0.30 MW
Rated Output DC Voltage from PV Array	0.63 kV
Power Flowing through the Breaker under Investigation	20 MW

The most important parameters of the PV system are summarized in Table 5.

3.2.2 Base Case Wind Power Network

The *Type 3 Wind Turbine Generator* [39] model provided from PSCAD comes with two different converter modeling options: average and detailed. Based on two different observations, the average converter model was shown to be sufficient for the purpose of this report.

The first observation is that the TRVs normally occur in microseconds after the current interruption, and thereby the dynamics of the wind generator and its controls can be ignored as they are too slow to react in this time interval [27].

The other observation was based on information from a technical specification document [41] provided with the model. This document states that the average converter model can be used when the focus is not on the effects of the produced harmonics or the firing controls. To verify this, the same TRV simulation was performed with the detailed and the average model and then compared. As the obtained graphs from these two simulations were identical, it was concluded that the average converter model was sufficient in the TRV study performed in this master thesis.

The grid-connected model of the Type 3 wind turbine (DFIG) is shown below in Figure 17. The 1320 pF stray capacitance placed at the terminal of the 22/0.69/0.9 kV transformer is the sum of the stray capacitance of a potential transformer, current transformer, lightening arrester, disconnector switch, and the transformer bushing.

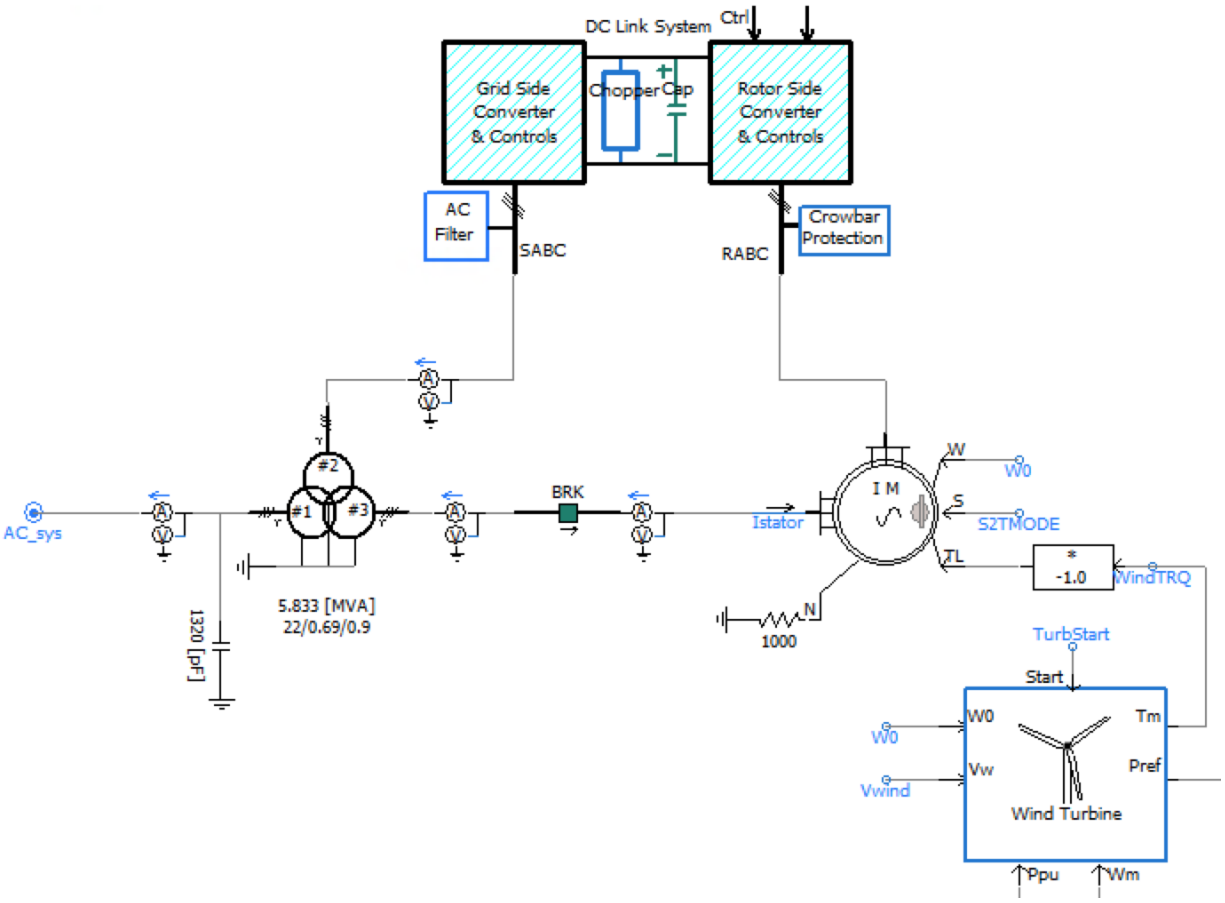

Figure 17: Type 3 wind power turbine model. The wind turbine can be connected to a 22 kV grid at the terminal to the left named AC_{sys}.

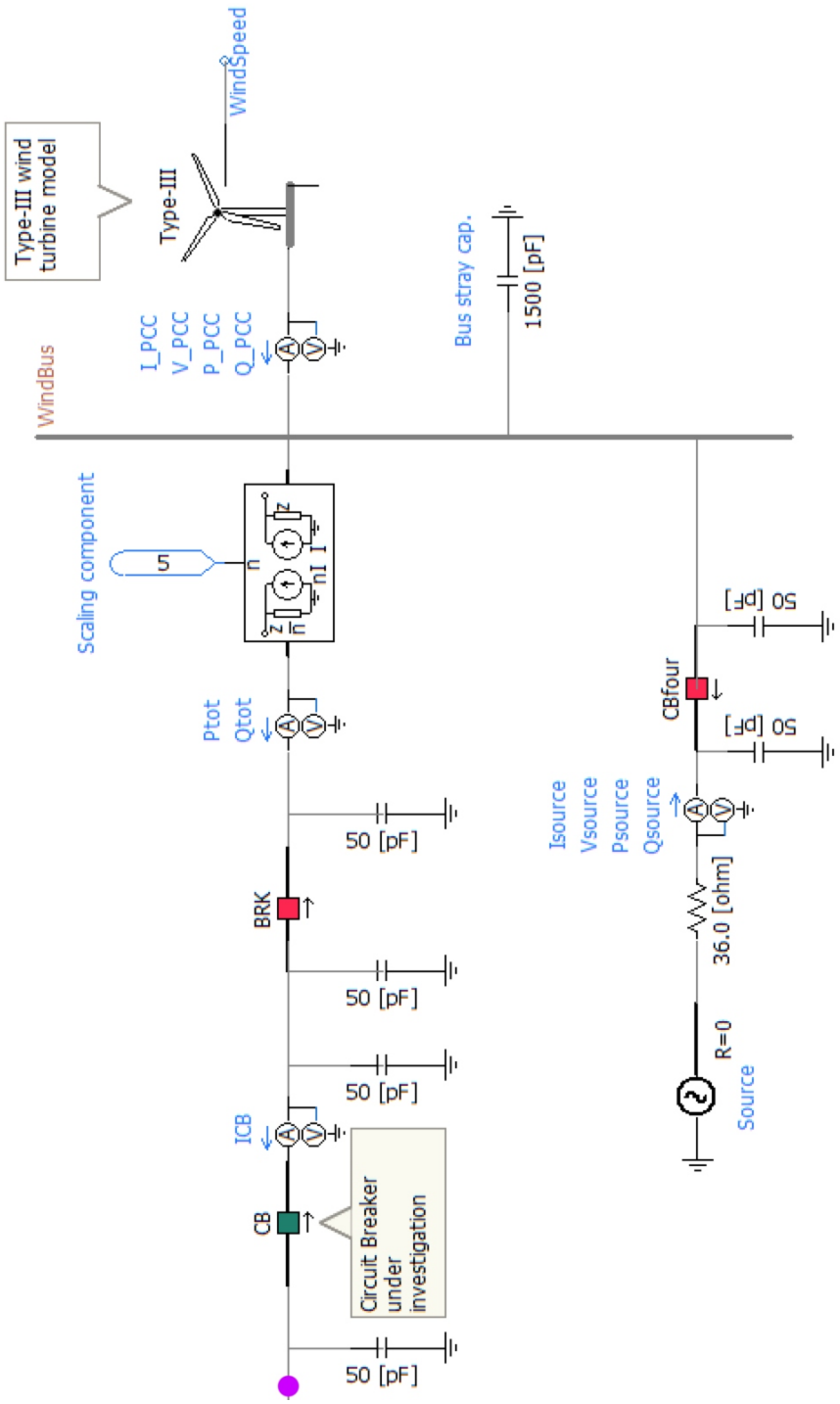

Figure 18: Part 1 of the total network used to simulate TRVs in the grid-connected wind power system.

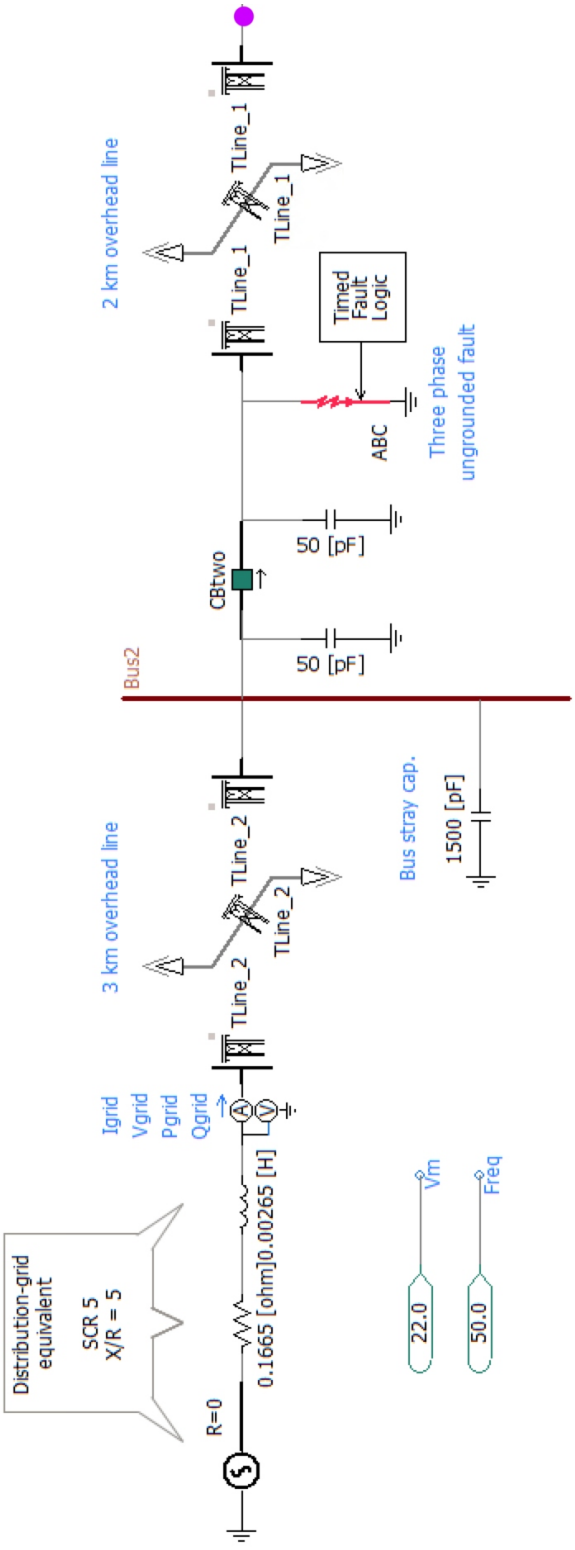

Figure 19: Part 2 of the total network used to simulate TRVs in the grid-connected wind power system.

In Figure 18 and Figure 19 part 1 and part 2 of the total base case wind power network are presented, respectively. In reality, these two parts are connected at the pink dots. The steady state values of the parameters listed above the multimeters are presented in Appendix I.

In this network the wind power plant is connected to a distribution grid through two overhead lines named *TLine_1* and *TLine_2*, of 2 km and 3 km respectively. In addition, at the bus named *WindBus*, an equivalent source to the one that was used in the PV system is connected. Since the *WindBus* has a voltage level of 22 kV while *PVBus* has a voltage level of 0.6 kV, a test circuit was made to decide the value of the resistance between the source and the *WindBus*. This was done to make sure that the effect of adding this source was similar in both of the base case networks. With the use of this test circuit, the resistance value which resulted in the same fault current contribution from the source used in the wind power network as the source used in the PV network was found. This resistance was found to be 36 Ω.

In similarity to the PV network, some power will be consumed by the source. With a scaling number of 5 it was possible to obtain 19.72 MW of real power flowing through the circuit breaker under investigation. This power deviates from the power flowing through the breaker under investigation in the PV base case network with 0.17 MW. As this deviation is small compared to the total amount of generated power it is assumed that it will not affect the general conclusions made in this study. The active power flowing through the breaker under investigation in both of the base case networks will be rounded up to 20 MW in the rest of the report for simplicity.

The circuit breaker under investigation is named *CB*. The same protection philosophy used in the PV case is used in the wind power case. When the fault occurs, it is assumed that *CB* is opening first, while the breaker named *CBtwo* is opening 200 ms after *CB* opens. The breaker named *BRK* belongs to the wind power plant model provided by PSCAD, and it is only used to connect the wind power plant to the rest of the grid at the start of the simulation. In similarity to the base case PV network presented above, the breaker named *CB* opens 43 ms after the short circuit occurred.

All the stray capacitance values used in the wind power base case network are presented in Table 4 in Section 2.5.

Table 6: Wind Power System Parameters

Parameter	Value
System Frequency	50 Hz
System Voltage	22 kV L-L, RMS
Rated Output Power from one Wind Turbine	5 MW
Power Flowing through the Breaker under Investigation	20 MW

The most important parameters of the wind power system are summarized in Table 6.

3.3 Network Components

In this section, each of the components used in the networks made in this thesis will be presented. The following components will be described: distribution grid equivalent, overhead line model, underground cable model, transformer model, circuit breaker model and the scaling component.

3.3.1 Distribution Grid Equivalent

In both of the base case networks, the same distribution grid equivalent is used. It was decided to use a relatively weak 22 kV grid with a short circuit ratio of 5. This short circuit ratio was chosen based on the study performed in [26]. The study performed in [26] investigated the TRVs caused by capacitor switching in a wind power plant that generated 12 MW connected to a grid with a short circuit ratio of 5.

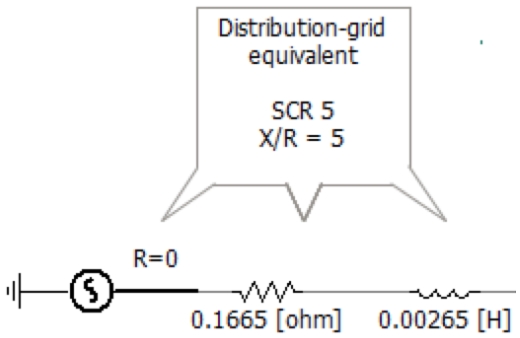

Figure 20: Distribution grid equivalent.

The distribution grid equivalent used in this thesis can be seen in Figure 20. This is a lumped representation of a distribution grid, which can be used in the type of TRV study that will be performed in this thesis [21]. The equivalent consists of a resistor of 0.1665 Ω, an inductor of 0.00265 H and an ideal source operating at an AC voltage of 22 kV line to line RMS. The ideal source has the ability to consume the active power delivered by the generating unit (wind or PV) and to generate reactive power consumed by the generating unit and the rest of the network if this is necessary. The SCR (or X/R ratio) of this distribution grid equivalent can be calculated as follows:

$$\frac{X}{R} = \frac{w * L}{R} = \frac{2 * \pi * 50Hz * 0.00265H}{0.1665\Omega} = 5$$

3.3.2 Overhead Line Model

The same overhead line model is used in both of the base case networks. The line geometry is presented in Figure 21. This is a travelling wave model chosen from the main library in PSCAD which is frequency dependent. The frequency dependent model represents all frequency-dependent effects of an overhead line and it is the most accurate time domain line model provided by PSCAD [38]. The grounding conductors (G1 and G2) shown in Figure 21 are grounded through a high impedance of 100 Ω*m assuming dry soil.

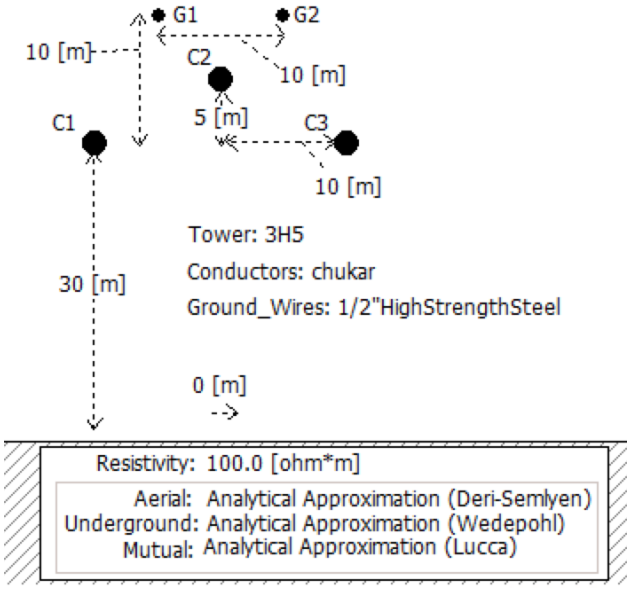

Figure 21: Overhead Line Model Geometry, from [38].

3.3.3 Underground Cable Model

In this subsection the underground cable used to investigate the effect of changing the overhead line (*TLine_1*) to a cable is presented. The geometry of the underground cable is presented in Figure 22. In similarity to the line model presented above, the frequency dependent model is also chosen for the cable modeling.

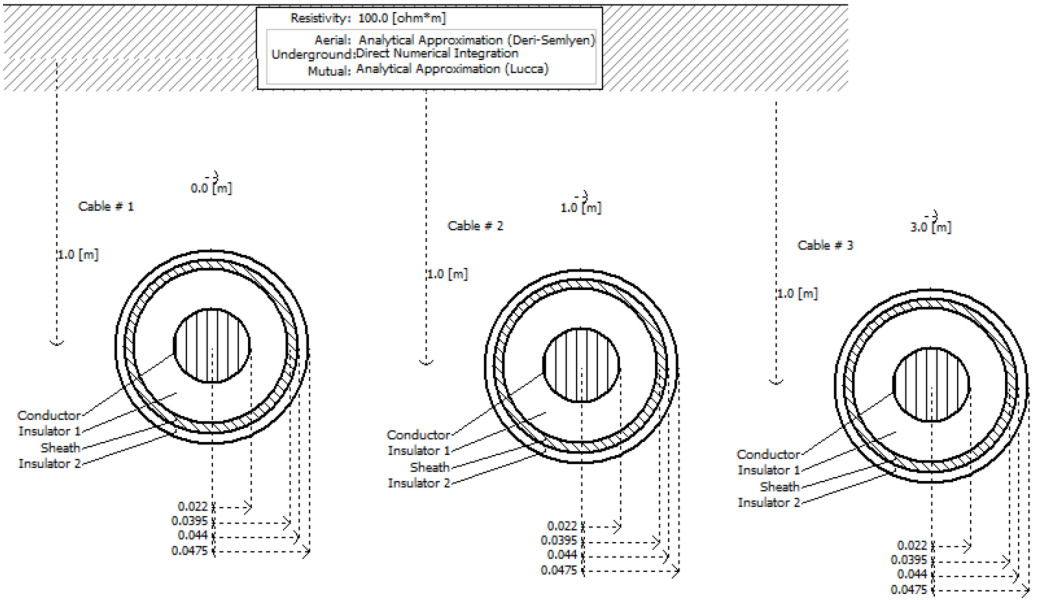

Figure 22: Underground Cable Model Geometry, from [38].

3.3.4 Transformer Model

A similar transformer model is used in both the PV network and the wind power network. The 3 phase 3 winding transformer presented in Figure 23 and Figure 24 is used in the wind power network, while the 3 phase 2 winding transformer presented in Figure 25 and Figure 26 is used in the PV network. Both of these transformer models provided from the PSCAD masters library are approved for TRV studies, and the three phase two winding transformer is for example also used in the TRV study performed in [42]. Both of the chosen transformers are based on the classical modeling approach, where inter-phase coupling is not represented. For the transformer used in the PV network it was chosen to have a delta-why coupling to reduce the harmonics produced by the photovoltaic plant.

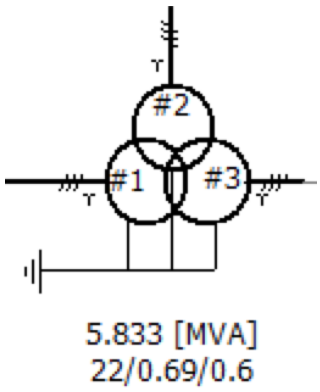

Figure 23: 3 phase 3 winding transformer used in the wind power network.

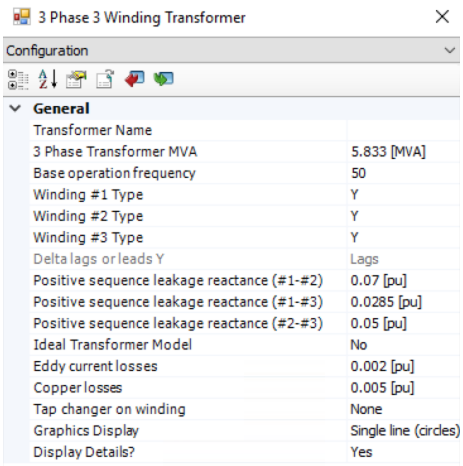

Figure 24: Details of the 3 phase 3 winding transformer used in wind power network.

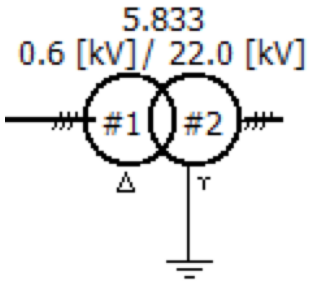

Figure 25: 3 phase 2 winding transformer used in the PV network.

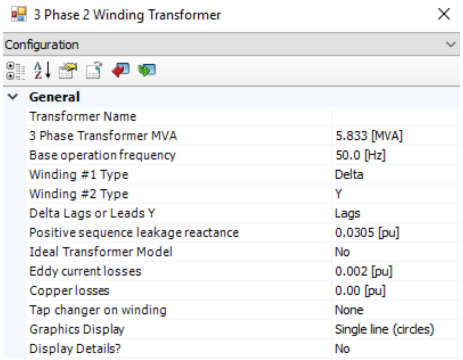

Figure 26: Details of the 3 phase 2 winding transformer used in PV network.

To make sure that the difference in the TRV observed in the PV network and in the wind power network was not caused by the different transformers used, it was desired to have these two transformers as similar as possible. With the use of trial and error on a test circuit, the leakage reactance of both of the transformers were chosen with the aim of having the same short circuit level in both of the transformers.

3.3.5 Circuit Breaker Model

As mentioned earlier, only the SF_6 and the vacuum breaker types are investigated in this thesis. The arc voltage of vacuum circuit breakers and medium voltage SF_6 circuit breakers are assumed to be low [2]. Based on the low arc voltage of the circuit breaker types under consideration, the switching arc is modelled as an ideal switch opening at current zero. Ideal in this case refers to a breaker with zero conductance in open position and zero resistance in closed and arcing states. In all the simulations performed in this thesis, the same circuit breaker model was used. The parameters of the chosen circuit breaker model are summarized below:

- Breaker open resistance: 1 MΩ
- Breaker closed resistance: 0 Ω
- Current chopping limit: 0 kA
- Arcing voltage: 0 kV

This circuit breaker model is used for the circuit breakers named *CB* and *CBtwo* in the base case networks presented in Section 3.2.1 and Section 3.2.2. These are the two circuit breakers located at each side of the fault in both of the base case networks.

3.3.6 Scaling Component

The only way to increase the power generated by the chosen wind farm is with the use of a scaling component. The scaling component is presented in Figure 27 and it is used to aggregate the windfarm from one wind turbine into several wind turbines.

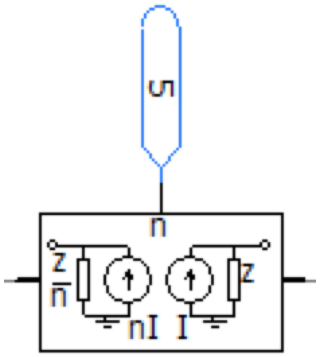

Figure 27: Scaling component with an aggregation number of 5.

This scaling component increases the power by taking the incoming current and times it with the aggregation number n. This is a way to model several wind turbines connected in parallel. In terms of capacitance and inductance, the scaling component can be seen as a π section, which means that it has a series inductor and parallel capacitors [41]. The inductance can be entered by the user, while the capacitance of the parallel capacitors is calculated within the component using (1) [41]:

$$C = \frac{(\Delta t)^2}{L} \tag{1}$$

Where Δt is the simulation time step in seconds and L is the inductance of the series inductor in H. For this scaling component to impact the study as less as possible the parameters of the scaling component was studied.

The total leakage reactance of the transformer connected to the scaling component is divided between the transformer and the scaling component. In the PV network, a 3 phase 2 winding transformer is used, with an original leakage reactance of 0.061 pu. To reduce the effect of the scaling component, the 0.061 pu leakage reactance was divided equally between the scaling component and the transformer which resulted in 0.0305 pu each. In the wind power network, a 3 phase 3 winding transformer were used, which resulted in a series reactance of 0.0305 pu in the scaling component and 0.07 pu for the 1-2 winding 0.0285 pu for the 1-3 winding and 0.05 pu for the 2-3 winding.

To obtain the correct total leakage reactance the same base values are used in the transformer and the scaling component. S_{base} was set to 5.833 MVA and V_{base} was set to 22 kV. The same base values are used in the PV and the wind power network to obtain the exact same scaling component. The inductance of the scaling component was calculated to 8.06 mH, for S_{base} = 5.833 MVA and V_{base} = 22 kV.

Concerning the capacitance, it is beneficial to have this as small as possible. As shown in Equation (1), a small C can be obtained by having a small time step and/or a large inductance. The time step has already been decided to 0.19 μs in Section 3.1.2. This time step is considered small, and reducing the time step any further results in a very slow simulation speed and a large memory will be needed to save the data. The capacitance is calculated by the use of Equation (1), with L = 8.06 mH and Δt = 0.19 μs:

$$C = \frac{(0.19 * 10^{-6} s)^2}{8.06 * 10^{-3} H} = 4.48 pF$$

The capacitance of the two capacitors of 4.48 pF each in the scaling component can be assumed not to affect the results of this study, as the 4.48 pF capacitors are small compared to the stray capacitances which are in the range of 50-1500 pF.

It should be mentioned that as opposed to the wind power case, it would have been possible to change the output power from the PV station without using the scaling component. This could have been done by increasing the voltage of the DC voltage source, and tuning the controllers and the LCL-filter to match the new rated power. However, to make the PV network and the wind power network as similar as possible, it was chosen to use the exactly same scaling component in the PV network as well. The only difference between the scaling component in the PV network and the wind power network is the number that the power is aggregated with. This number does not affect the parameters of the scaling component, as the parameters of the scaling component only depend on the chosen reactance and the time step.

3.4 Special Case Scenarios

It is known from a previous study that a small change in some of the network parameters might decide whether or not the breaker under investigation is operating beyond its limit [21]. Consequently, it is essential to investigate different case scenarios with distributed generation to check whether or not the circuit breakers are operating beyond their limits in the case of distributed generation.

In this thesis, four different parameters that might affect the transient recovery voltage resulting from a short line fault will be investigated. The same parameters will be investigated in both the photovoltaic network and the wind power network. The four different parameters that will be examined are:

- Different lengths of the overhead line (*TLine_1*) between the fault and the circuit breaker under investigation.
- Changing the overhead line (*TLine_1*) between the fault and the circuit breaker under investigation to a cable (*Cable_1*). Investigating the effect of changing the length of this cable.
- Changing the power flowing through the breaker under investigation.
- Changing the time between the short circuit instant and the breaker contacts separation.

The explanation to why exactly these four parameters where chosen is based on observations from simulations performed in the project thesis presented in [1]. From the theory, high RRRVs are expected in the case of a short line fault in an overhead line network. The RRRV is among other parameters dependent on the length of the line. In addition, it will be interesting to see the difference in the TRV caused in a cable system compared to a line system, as cables are frequently used in distribution systems. Consequently, different possible line and cable lengths should be investigated with the purpose of finding the worst case scenarios.

In addition, it is known from previous studies that the generated power from the distributed generation unit will affect the short circuit current level [18, 19, 25]. Different short circuit levels through the circuit breaker are expected to affect the transient recovery voltages [21]. In addition, the most demanding case may occur at different fault current levels depending on the design of the breaker [2].

The time from the short circuit occurrence until the breaker contacts separation will also affect the transient recovery voltage. This is among other things due to the decaying DC component of the short circuit current that will result in a different short circuit level for different time instants after the fault occurred. As the transient recovery voltage depends on the short circuit current, different levels of short circuit current will affect the transient recovery voltage.

3.4.1 Different Lengths of the Overhead Line *TLine_1*

In Table 7 the different case scenarios used to investigate the effect of changing the length of the overhead line (*TLine_1*) are presented. Since short line faults occur at a distance of a few hundred meters to a few kilometers away from the circuit breaker [2, 31], all of the chosen line lengths are kept inside this range.

Table 7: Different case scenarios used to investigate the effect of changing the length of *TLine_1*.

Case scenario Number	Case Description
1	TLine_1 = 0.6 km
2	TLine_1 = 0.8 km
3	TLine_1 = 1 km
4	TLine_1 = 2 km (base case)
5	TLine_1 = 3 km
6	TLine_1 = 5 km

The only change that is made to the base case networks presented in Section 3.2.1 and Section 3.2.2 is the length of the line named *TLine_1*.

3.4.2 Changing the Overhead Line (*TLine_1*) to an Underground Cable (*Cable_1*)

In Table 8 the different case scenarios used to investigate the effect of changing the overhead line to a cable are presented. In similarity to the case described above with different lengths of the overhead line (*TLine_1*), the chosen lengths of the cable (*Cable_1*) are kept inside the typical range of short line faults.

Table 8: Different case scenarios used to investigate the effect of changing the length of *Cable_1*.

Case scenario Number	Case Description
7	Cable_1 = 0.6 km
8	Cable_1 = 0.8 km
9	Cable_1 = 1 km
10	Cable_1 = 2 km
11	Cable_1 = 3 km
12	Cable_1 = 5 km

The only change that is made to the base case networks presented in Section 3.2.1 and Section 3.2.2 is replacing the overhead line *TLine_1* by an underground cable (*Cable_1*) of different lengths. This will result in a system with one cable (*Cable_1*) and one overhead line (*TLine_2*). Since the circuit

breaker under investigation is not directly connected to the line, the breaker class S1 (cable system) is used [22].

3.4.3 Changing the Power Flowing through the Breaker

In Table 9 the different case scenarios used to investigate the effect of changing the power flowing through the breaker under investigation are presented.

Table 9: Different case scenarios used to investigate the effect of changing the power flowing through the breaker.

Case scenario Number	Case Description
13	5 MW active power flowing through the breaker
14	9 MW active power flowing through the breaker
15	13 MW active power flowing through the breaker
16	20 MW active power flowing through the breaker (base case)

Regarding the simulations of case scenario 13-16 performed on the photovoltaic base case network and the wind power base case network only the aggregation number in the scaling component had to be changed. As mentioned earlier, due to the source connected at the bus closest to the PV plant in the PV network, not all of the power generated by the PV system will flow through the circuit breaker under investigation. This observation is also valid for the wind power network. In the photovoltaic network, it was possible to get 4.82 MW, 9.22 MW, 13.33 MW and 19.89 MW flowing through the breaker under investigation. In the wind power network it was possible to get 4.84 MW, 9.32 MW, 13.33 MW and 19.72 MW flowing through the breaker under investigation. Since the deviations between the generated power in the wind and PV networks are small compared to the total amount of generated power it was decided to round these numbers to the closest integer for simplicity.

3.4.4 Changing the Time between the Short Circuit Instant and the Breaker Contacts Separation.

Different scenarios used to investigate the effect of changing the time from the short circuit instant until breaker contacts separation are presented in Table 10.

Table 10: Different case scenarios used to investigate the effect of changing the time between short circuit and breaker contact separation.

Case scenario Number	Case Description
17	43 ms between short circuit and breaker contact separation (base case)
18	63 ms between short circuit and breaker contact separation
19	83 ms between short circuit and breaker contact separation
20	103 ms between short circuit and breaker contact separation

These four values were chosen based on the following explanation. When a short circuit occurs, the time until the breaker contacts are separating will be the sum of the activation time of an overcurrent device and the opening time of the circuit breaker. The minimum activation time of an overcurrent device is one half-period of the rated frequency, i.e. 10 ms in a 50 Hz system [24]. The maximum relay time is assumed to be around 43 ms.

For the circuit breakers studied in this thesis, the minimum opening time is assumed to be 33 ms, while the maximum opening time is assumed to be 60 ms. This is shown in Table 3 in Section 2.4.

On the basis of this, the minimum time from the short circuit occurs and until the breaker contacts are opening is set to 10 + 33 = 43 ms, which is used in case scenario 17. The maximum time from the short circuit instant and until contact separation is set to 43 + 60 = 103 ms, which is used in scenario 20. In addition to the minimum and the maximum time, two time instants between these two values were also chosen.

Regarding the simulations of case scenario 17-20, only the time of the breaker operation of the two circuit breakers named *CB* and *CBtwo* has to be changed.

It is assumed that the circuit breaker under investigation (CB) opens as described in Table 10, while *CBtwo* opens 200 ms later. In this way the fault instant is kept the same, and the time between the short circuit and the breaker contact separation is decided by the opening instant of the circuit breakers. As mentioned earlier, it is assumed that the circuit breakers in each of the three phases are opening at the same time, which is normal practice in distribution systems [26].

4 Results and Discussion

Simulations of 20 case scenarios have been performed on the two different base case networks presented in the previous chapter. In this chapter, the results and the following discussion of the 20 case scenarios are presented. The simulation results of the photovoltaic network and the wind power network are presented in two separate sections and then compared. Finally, some possible sources of errors will be discussed.

The steady state results for both the wind and the PV base case networks can be found in Appendix I. Steady state occurs at different time instants for the PV and the wind power system, at around 2.5 sec and around 2 sec respectively. In addition, to reduce the simulation time it was desirable to apply the fault as early as possible. On the basis of this, the fault instant is different for the photovoltaic and the wind power network.

4.1 Simulation Results for the Photovoltaic Network

Simulations of a three phase ungrounded fault has been performed on the photovoltaic network presented in Section 3.2.1. The result from the base case network and each of the 20 case scenarios are presented and discussed below.

4.1.1 Base Case Photovoltaic Network

The simulation results from the PV base case network are presented in this subsection.

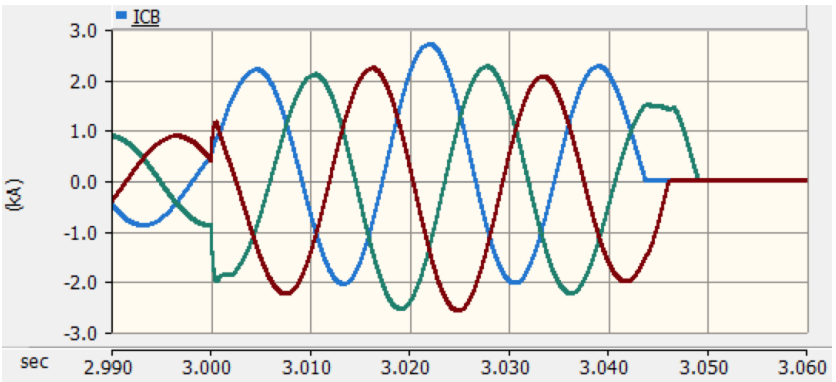

Figure 28: Current through the circuit breaker under investigation from the fault instant to the current interruption.

In Figure 28 the fault current through the breaker under investigation is presented. The peak value of the current is 2.71 kA. Since this value is between 10 % and 30 % of the total breaking capacity of 25 kA, the T30 capability curves should be used in this case. In addition, it can be observed that the fault occurs at 3.0 sec, and the current is interrupted at around 3.0436 sec, 3.0460 sec and 3.0490 sec, for the first, second and third pole to clear, respectively.

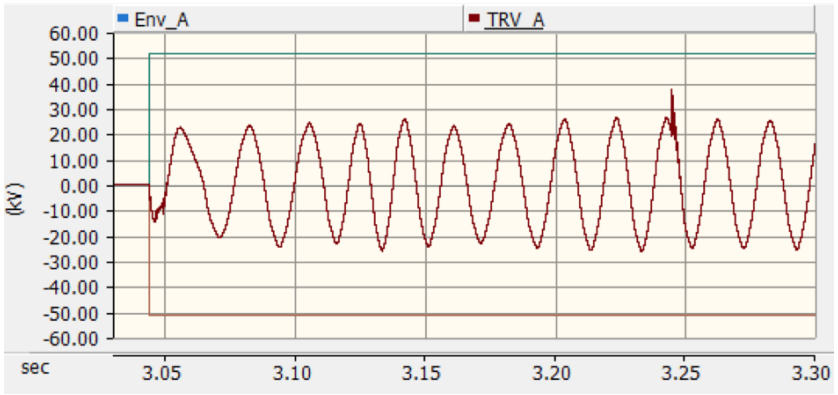

Figure 29: TRV for the first pole to clear showing the time instant when the fault is isolated.

In Figure 29 the TRV for the first pole to clear is shown for a time period of 300 ms. It can be observed that the circuit breaker under investigation is interrupting the current at around 3.043 sec, while the circuit breaker at the other side of the fault is isolating the fault from the network at around 3.243 sec. This observation corresponds to the protection philosophy discussed in section 3.2.1, where it was mentioned that the second circuit breaker has to wait 200 ms to check if the fault was cleared by the first circuit breaker opening. Another observation that should be made from Figure 29 is the values of the capability curves (green and orange). These are the T30 capability curves for class S2 circuit breakers rated 24 kV, which both has an amplitude of 51.2 kV, and a steepness of 3.01 kV/μs as shown in Table 2 in Section 2.3. By investigating Figure 29 it can be observed that the peak of the TRV is kept within the capability curves at all times.

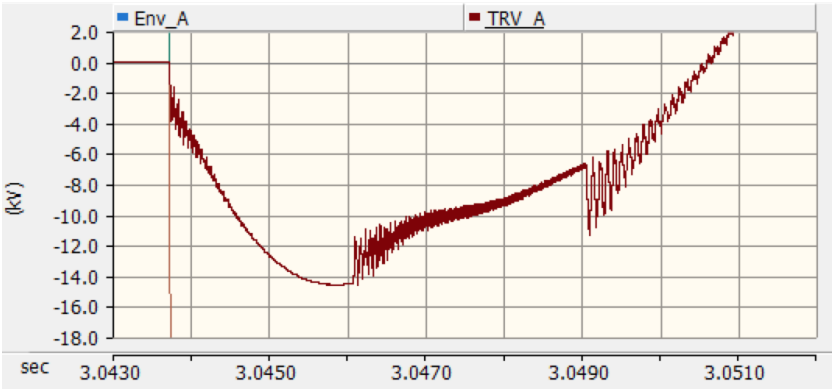

Figure 30: TRV for the first pole to clear showing the time instants where second and third pole are clearing.

In Figure 30 a zoomed version of the TRV presented in Figure 29 is shown. It can be observed that new transients are occurring at around 3.0460 sec and around 3.0490 sec. These are the time instants when the second and third pole are cleared, and the new transients are caused by a dependency between the phases.

This dependency is probably caused by the coupling between the conductors in the line/cable. When one phase opens a transient occurs on that phase which can further induce transients in the other phases.

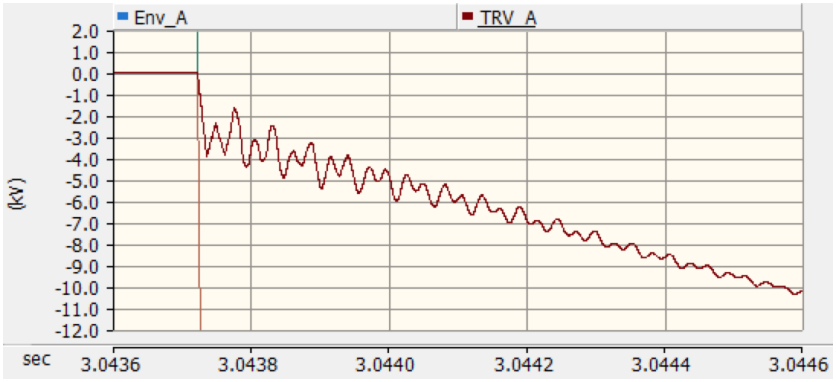

Figure 31: TRV for the first pole to clear.

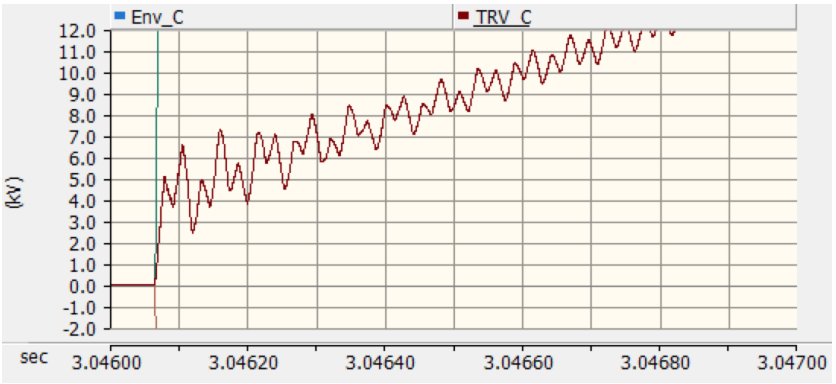

Figure 32: TRV for the second pole to clear.

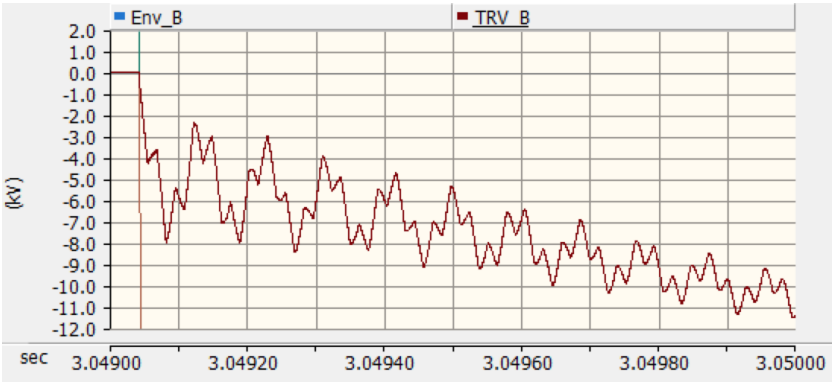

Figure 33: TRV for the third pole to clear.

A closer picture of the TRV for the first, second and third pole to clear are presented in Figure 31, Figure 32 and Figure 33, respectively. It can be observed that the shape of these three TRVs are somehow similar, but the oscillations are damped faster out in the first pole to clear compared to the second and third.

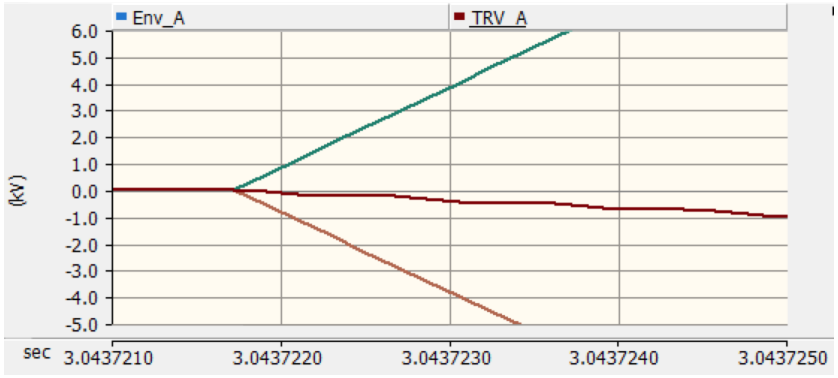

Figure 34: RRRV for the first pole to clear for a current chopping limit of 0 A.

In Figure 34 the RRRV for the first pole to clear is shown. It can be observed that the RRRV is not very steep compared to the T30 capability curves which has a slope of 3.01 kV/μs. The RRRV is measured to 0.437 kV/μs.

In all the TRV results presented above, a current chopping limit of 0 A is used. In Figure 35 and Figure 36 the RRRV and the TRV for the first pole to clear for a current chopping limit of 5 A are shown.

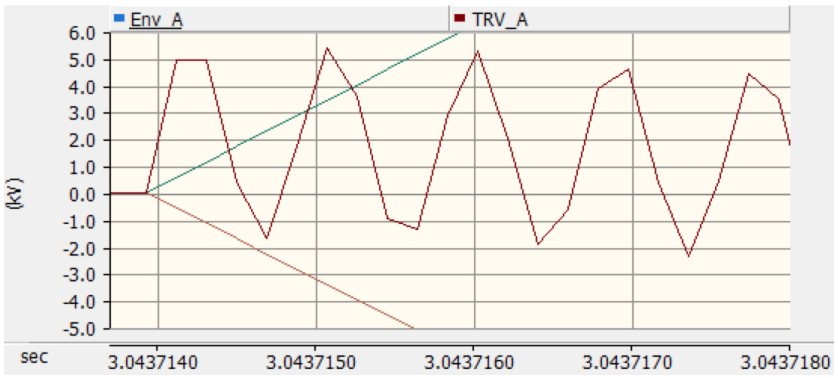

Figure 35: RRRV for the first pole to clear for a current chopping limit of 5 A.

In Figure 35 the RRRV is shown for a current chopping of 5 A. In this case the RRRV is so steep that the T30 capability curve is exceeded at 3.0437139 sec.

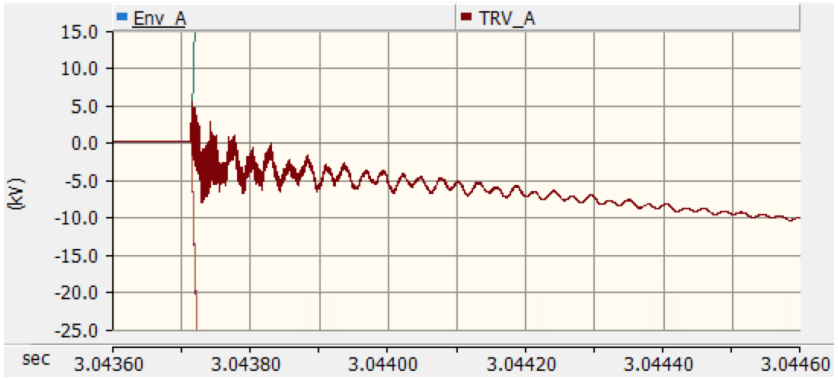

Figure 36: TRV for the first pole to clear for a current chopping limit of 5 A.

In Figure 35 it can be observed that very high frequent oscillations occur right after the current is interrupted. The current chopping level for modern vacuum circuit breakers is in the range of 3.5 - 25 A [2]. In the simulations it was observed no significant overvoltage for a current chopping limit higher than 0 A, and for simplification in the simulations it was set to 0 A. Consequently, a current chopping limit of 0 A is used for all the case scenario simulations performed in this report.

4.1.2 Case Scenario 1-6. Different Lengths of the Overhead Line *TLine_1*

Simulations of case scenario 1-6 have been performed on the photovoltaic network described in Section 3.4.1.

Table 11: RRRV for case scenario 1-6.

Case scenario	**RRRV 1. pole to clear [kV/μs]**	**RRRV 2. pole to clear [kV/μs]**	**RRRV 3. pole to clear [kV/μs]**
1: Line 0.6 km	0.467	0.658	0.485
2: Line 0.8 km	0.591	0.568	0.624
3: Line 1 km	0.450	0.566	0.507
4: Line 2 km (base case)	0.437	0.574	0.483
5: Line 3 km	0.417	0.517	0.404
6: Line 5 km	0.391	0.446	0.263

In Table 11 the RRRVs for the first, second and third pole to clear for case scenario 1-6 are presented. The fault current for the line of 5 km is below 10 % of the breaking capacity, so the T10 capability curve is used for this line length. For all the other chosen line lengths the T30 capability curve is used. The T10 capability curve has a steepness of 3.11 kV/μs while the T30 curve has a steepness of 3.01 kV/μs. It can be observed that none of the values in Table 11 are steeper than the relevant capability curve. By comparing the RRRVs for the different line lengths, it can be noticed that the steepest RRRV measured is 0.658 kV/μs, which is observed in the second pole to clear for a line of 0.6 km. The lowest RRRV has a value of 0.263 kV/μs, and it is observed in the third pole to clear for a line of 5 km.

The trend that can be observed in Table 11 is that the steepest RRRV is observed for the second pole to clear. This observation is valid for all the chosen line lengths except for the line of 0.8 km. It can also be noticed that the steepest RRRVs are observed in the shortest chosen line lengths.

Table 12: TRV peak for case scenario 1-6.

Case scenario	**TRV peak 1. pole to clear [kV]**	**TRV peak 2. pole to clear [kV]**	**TRV peak 3. pole to clear [kV]**
1: Line 0.6 km	13.83	20.45	22.27
2: Line 0.8 km	13.97	20.42	21.89
3: Line 1 km	14.11	20.39	21.50
4: Line 2 km (base case)	14.67	20.36	19.68
5: Line 3 km	14.81	20.04	18.15
6: Line 5 km	16.61	19.01	16.28

In Table 12 the TRV peaks are shown for the first, second, and third pole to clear for case scenario 1-6. The T10 capability curve is used for the 5 km line while the T30 capability curve is used for all the other line lengths. The T10 capability curve has a peak of 52.9 kV while the T30 curve has a peak value of 51.2 kV. The highest TRV peak is observed in the third pole to clear for a line of 0.6 km, and has a value of 22.27 kV. The lowest TRV peak is measured to 13.83 kV, and is observed in the first pole to clear for the 0.6 km line. None of the TRV peak values observed in case scenario 1-6 are exceeding the relevant capability curve.

The trend that can be observed is that the highest TRV peak for the shortest three lengths is found in the third pole to clear. On the other hand, for the longest three line lengths the highest peak is observed in the second pole to clear. In addition, the TRV peak for the second and third pole to clear are decreasing with an increasing line lengths. However, the TRV peak of the first pole to clear is increasing with an increased line length.

4.1.3 Case Scenario 7-12. Changing the Overhead Line (*TLine_1*) to an Underground Cable (*Cable_1*)

Simulations of case scenario 7-12 have been performed on the photovoltaic network described in Section 3.4.2.

Table 13: RRRV for case scenario 7-12.

Case scenario	**RRRV 1. pole to clear [kV/μs]**	**RRRV 2. pole to clear [kV/μs]**	**RRRV 3. pole to clear [kV/μs]**
7: Cable 0.6 km	0.240	0.508	0.245
8: Cable 0.8 km	0.292	0.336	0.287
9: Cable 1 km	0.306	0.474	0.322
10: Cable 2 km	0.231	0.331	0.238
11: Cable 3 km	0.228	0.309	0.239
12: Cable 5 km	0.208	0.445	0.216

In Table 13 the RRRVs for the first, second and third pole to clear for case scenario 7-12 are shown. Even though the peak of the fault current is changed when the cable length is changed, the fault current was kept between 10 % and 30 % of the breaking capacity for all the chosen cable lengths. The T30 capability curve of a class S1 breaker rated 24 kV has a value of 2.47 kV/μs as showed in Table 1 in Section 2.3. It can be observed that none of the RRRVs in Table 13 are exceeding this value. The steepest RRRV measured is 0.508 kV/μs, and it is observed in the second pole to clear for a cable of 0.6 km. The lowest RRRV is measured to 0.208 kV/μs, and it is observed in the first pole to clear for a cable of 5 km.

In similarity to the line case presented above, a steeper RRRV is expected for smaller cable lengths. This phenomena is observed in Table 13, as the steepest RRRV was observed in the shortest cable length while the lowest RRRV is observed in the longest cable length. This observation is probably

because the fault current is increased for a decreasing cable length. Increasing the short circuit current could contribute to a higher RRRV [27, 30, 31].

By comparing the RRRVs observed in the cable case to the RRRVs observed in the line case in Table 11, it can be observed that the RRRVs in the line cases are in general steeper than the RRRVs observed in the cable cases. This is a result of the higher wave impedance in the line compared to the cable.

Table 14: TRV peak for case scenario 7-12.

Case scenario	**TRV peak 1. pole to clear [kV]**	**TRV peak 2. pole to clear [kV]**	**TRV peak 3. pole to clear [kV]**
7: Cable 0.6 km	14.18	20.17	23.30
8: Cable 0.8 km	14.02	20.08	23.16
9: Cable 1 km	13.87	19.98	22.99
10: Cable 2 km	13.18	19.54	22.03
11: Cable 3 km	13.03	19.14	21.03
12: Cable 5 km	13.13	18.42	19.62

The TRV peaks for the first, second, and third pole to clear for case scenario 7-12 are presented in Table 14. The T30 capability curve for an S1 breaker rated 24 kV has a peak value of 47.0 kV as presented in Table 1 in Section 2.3. It can be noticed that none of the values in Table 14 are exceeding the capability of the breaker. The highest TRV peak is measured to 23.30 kV in the third pole to clear for a cable of 0.6 km. The lowest TRV peak is measured to 13.03 kV in the first pole to clear for a cable of 3 km.

The trend that can be observed in Table 14 is that for each of the poles to clear the TRV peak decreases with an increasing cable length. In addition, for all the chosen cable lengths, the highest TRV peak is observed in the third pole to clear.

4.1.4 Case Scenario 13-16. Changing the Power Flowing through the Breaker

Simulations of case scenario 13-16 have been performed on the photovoltaic network described in Section 3.4.3.

Table 15: RRRV for case scenario 13-16.

Case scenario	**RRRV 1. pole to clear [kV/μs]**	**RRRV 2. pole to clear [kV/μs]**	**RRRV 3. pole to clear [kV/μs]**
13: 5 MW flowing through the breaker	0.242	0.382	0.266
14: 9 MW flowing through the breaker	0.346	0.382	0.298
15: 13 MW flowing through the breaker	0.367	0.493	0.379
16: 20 MW flowing through the breaker (base case)	0.437	0.574	0.483

In Table 15 the RRRVs for the first, second and third pole to clear for case scenario 13-16 are presented. Due to the reduction in power generated, the fault current is below 10 % of the rated breaking capacity for case scenario 13-15. Based on this, the T10 capability curves should be used in case scenario 13-15. The T10 capability curve has a steepness of 3.11 kV/μs as presented in Table 2 in Section 2.3. It can be observed that none of the case scenarios presented in Table 15 results in a situation where the RRRV is exceeding the capability of the breaker. Scenario 13-15 does not exceed the T10 capability curve of 3.11 kV/μs, while case scenario 16 does not exceed the T30 capability curve of 3.01 kV/μs.

The trend that can be observed in Table 15 is that for each of the poles to clear the steepness of the RRRV increases with an increasing power flow. This is probably related to the increased fault current for higher power flows which can contribute to steeper RRRVs [27, 30, 31]. In addition, the steepest RRRV for each of the chosen power flows is observed in the second pole to clear.

Table 16: TRV peak for case scenario 13-16.

Case scenario	**TRV peak 1. pole to clear [kV]**	**TRV peak 2. pole to clear [kV]**	**TRV peak 3. pole to clear [kV]**
13: 5 MW flowing through the breaker	15.36	18.69	23.68
14: 9 MW flowing through the breaker	14.02	19.37	22.40
15: 13 MW flowing through the breaker	13.01	19.90	21.32
16: 20 MW flowing through the breaker (base case)	14.67	20.36	19.68

In Table 16 the TRV peaks for the first, second and third pole to clear for case scenario 13-16 are presented. As mentioned above, the T10 capability curve should be used for case scenario 13-15. The peak value of the T10 capability curve for class S1 circuit breakers is 52.9 kV, while the peak value of the T30 capability curve is 51.2 kV.

It can be observed that none of the values in Table 16 are exceeding the relevant capability curve. The highest measured TRV peak is 23.68 kV, which is measured in the third pole to clear for a power flow of 5 MW. The lowest TRV peak is observed in the first pole to clear for a generated power of 13 MW, and is measured to 13.01 kV.

4.1.5 Case Scenario 17-20. Changing the Time between the Short Circuit Instant and the Breaker Contacts Separation.

Simulations of case scenario 17-20 have been performed on the photovoltaic network presented in Section 3.4.4.

Table 17: RRRV for case scenario 17-20.

Case scenario	**RRRV 1. pole to clear [kV/μs]**	**RRRV 2. pole to clear [kV/μs]**	**RRRV 3. pole to clear [kV/μs]**
17: 43 ms between short circuit and contact separation (base case)	0.437	0.574	0.483
18: 63 ms between short circuit and contact separation	0.317	0.291	0.457
19: 83 ms between short circuit and contact separation	0.213	0.322	0.440
20: 103 ms between short circuit and contact separation	0.329	0.652	0.535

In Table 17 the RRRVs for the first, second and third pole to clear for case scenario 17-20 are presented. The steepest RRRV is measured to 0.652 kV/μs, and is observed in the second pole to clear for 103 ms between the short circuit and the contact separation. The lowest RRRV is observed in the first pole to clear for 83 ms between the short circuit and the contact separation, and is measured to 0.213 kV/μs. None of the values are exceeding the T30 capability curve of the breaker which has a steepness of 3.01 kV/μs.

The trend that can be observed in Table 17 is that the steepest RRRVs are observed for the shortest and the longest chosen time instants. By investigating the fault current is was observed that the peak was higher for 43 ms and 103 ms compared to 63 ms and 83 ms. The difference in peak of the fault current could explain the observations presented in Table 17.

Table 18: TRV peak for case scenario 17-20.

Case scenario	TRV peak 1. pole to clear [kV]	TRV peak 2. pole to clear [kV]	TRV peak 3. pole to clear [kV]
17: 43 ms between short circuit and contact separation (base case)	14.67	20.36	19.68
18: 63 ms between short circuit and contact separation	16.20	23.80	23.35
19: 83 ms between short circuit and contact separation	13.78	23.20	20.06
20: 103 ms between short circuit and contact separation	22.55	35.81	31.41

The TRV peak values for the first, second and third pole to clear for case scenario 17-20 are presented in Table 18. The highest TRV peak is measured to 35.81 kV, and is observed in the second pole to clear for 103 ms between the short circuit and the breaker contact separation. The lowest TRV peak is observed in the first pole to clear for 83 ms between the short circuit and the breaker contact separation, and is measured to 13.78 kV. All the values in Table 18 are within the T30 capability curve of the breaker which is 51.2 kV.

The trend that can be observed in Table 18 is that the highest TRV peak is observed in the second pole to clear for all the chosen time instants.

4.2 Simulation Results for the Wind Power Network

Simulation of a three phase ungrounded fault has been performed on the wind power network presented in Section 3.2.2. The results from the wind power base case network and each of the 20 case scenarios are presented and discussed below.

4.2.1 Base Case Wind Power Network

The simulation results from the wind power base case network are presented in this subsection.

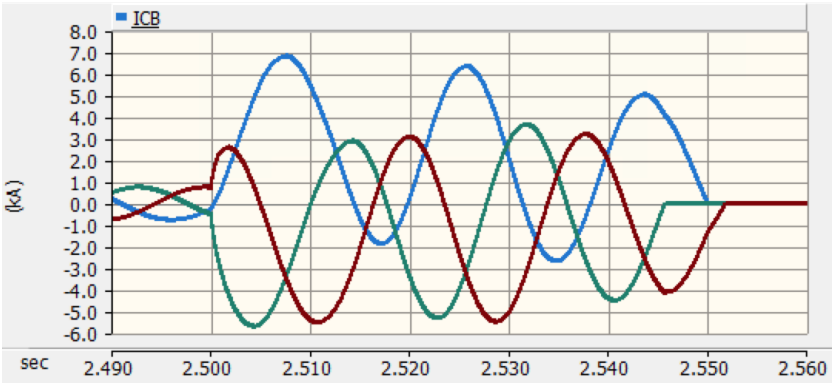

Figure 37: Fault current through the circuit breaker under investigation.

In Figure 37 the fault current through the breaker under investigation is presented. The peak value of the current is 6.83 kA. In similarity to the PV case, the fault current is between 10 % and 30 % of the total breaking capacity of 25 kA. Based on this, the T30 capability curves should be used in this case.

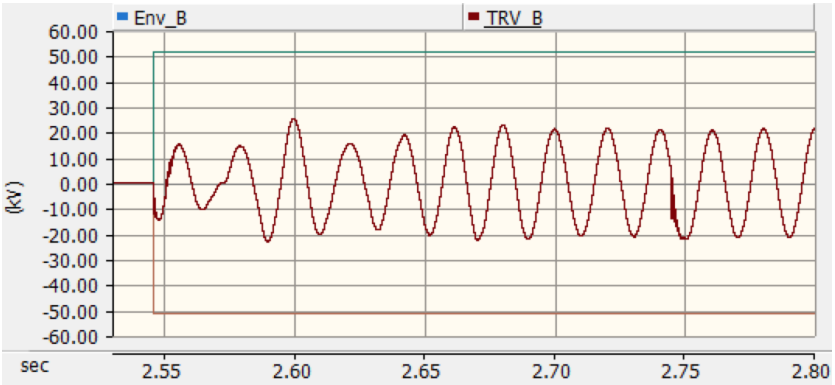

Figure 38: TRV for the first pole to clear showing the time instant when the fault is isolated.

In Figure 38 the TRV for the first pole to clear for is showed for a time period of 300 ms. The first breaker clears the current at around 2.543 sec, while the second breaker isolates the fault at around 2.743 sec. The green and the orange curves are the T30 capability curves which both have a steepness of 3.01 kV/μs and an amplitude of 51.2 kV as shown in Table 2 in section 2.3.

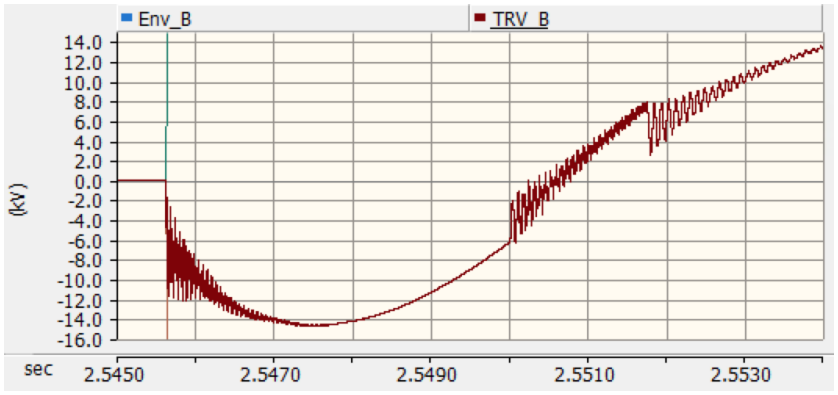

Figure 39: TRV for the first pole to clear showing the time instants where the second and the third pole are clearing.

In Figure 39 a zoomed version of the TRV presented in Figure 38 is shown. In similarity to the PV case, a dependency between the phases can be observed. This is observed by noticing that new transients occur at around 2.55000 sec and around 2.55175 sec, which are the time instants when the second and third pole are clearing.

This dependency is probably caused by a combination of the coupling between the conductors in the line/cable and the neutral voltage variation of the wind turbine. The neutral of the induction machine used in the DFIG is grounded through a high resistance (1000 Ω). When one phase opens the system become unbalanced and neutral voltage can change which influences the voltages on the other phases consequently.

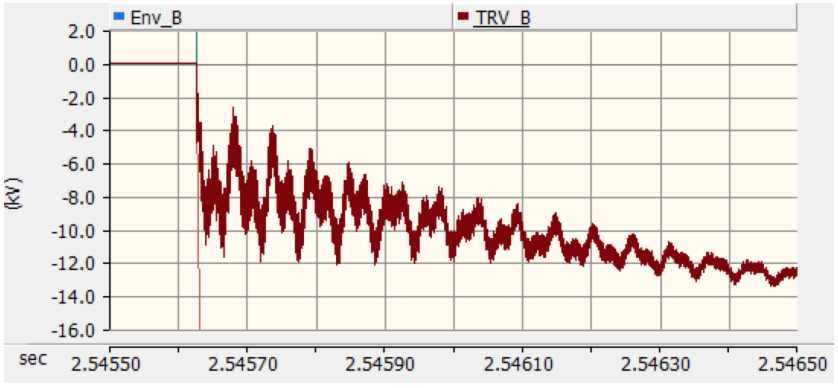

Figure 40: TRV for the first pole to clear.

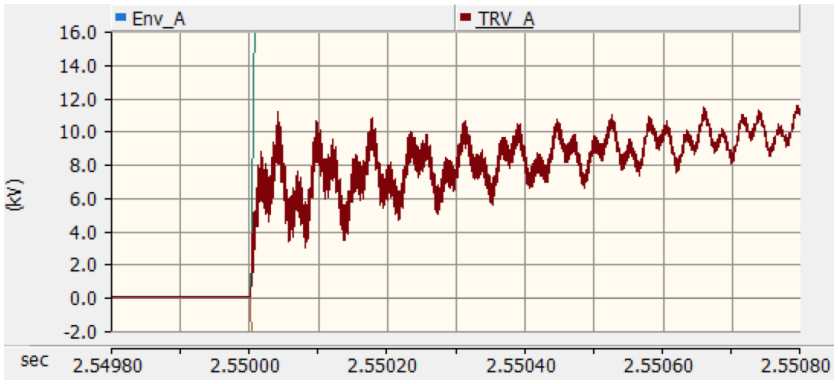

Figure 41: TRV for the second pole to clear.

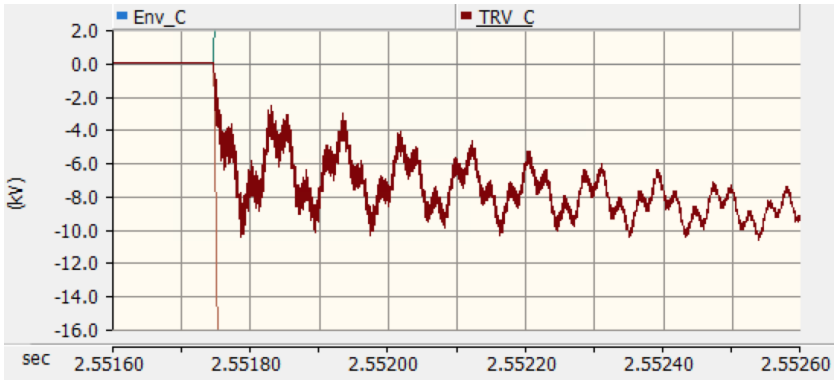

Figure 42: TRV for the third pole to clear.

In Figure 40, Figure 41 and Figure 42 the TRVs for the first, second and third pole to clear are presented. It can be observed that all of the TRVs have many high frequent oscillations. In addition, it can be observed that all of the TRVs consist of several different frequencies.

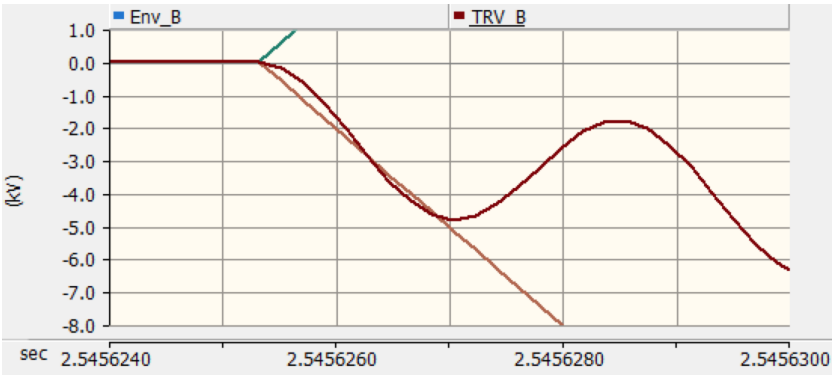

Figure 43: RRRV (red) for the first pole to clear.

In Figure 43 the RRRV for the first pole to clear is presented. It can be observed that the RRRV (red) is exceeding the T30 capability curve (orange) at 2.54562620 sec. The RRRV is measured to 3.086 kV/μs which is steeper than the capability curve of 3.01 kV/μs.

4.2.2 Case Scenario 1-6. Different Lengths of the Overhead Line *TLine_1*

Simulations of case scenario 1-6 have been performed on the wind power network described in Section 3.4.1.

Table 19: RRRV for case scenario 1-6.

Case scenario	**RRRV 1. pole to clear [kV/μs]**	**RRRV 2. pole to clear [kV/μs]**	**RRRV 3. pole to clear [kV/μs]**
1: Line 0.6 km	3.167	2.446	1.768
2: Line 0.8 km	3.012	2.916	2.996
3: Line 1 km	3.065	2.360	1.897
4: Line 2 km (base case)	3.086	2.291	1.758
5: Line 3 km	3.042	2.308	1.613
6: Line 5 km	2.440	1.817	1.327

In Table 19 the RRRVs for the first, second and third pole to clear for case scenario 1-6 are presented. For a line length of 0.6 km and 0.8 km the fault current is between 30 % and 60 % of the rated capacity so the T60 capability curves are used for these line lengths. For all the other chosen line lengths

the relevant capability curve is the T30. The steepness of the T60 capability curve is 1.67 kV/μs while the steepness of the T30 capability curve is 3.01 kV/μs. The values marked with red are the RRRVs that exceed the relevant capability curve.

It can be observed that the steepest RRRV is found in the first pole to clear for each of the line lengths. By comparing all the RRRVs in Table 19 it can be observed that the steepest RRRV measured is 3.167 kV/μs. The steepest RRRV is measured in the first pole to clear for a line of 0.6 km. The lowest RRRV is measured to 1.327 kV/μs in the third pole to clear for a line length of 5 km.

In similarity to the results from case scenario 1-6 performed on the PV network, the steepest RRRV is observed in the shortest chosen line length. This might be caused by the increased fault current for the shorter line lengths. Increasing the current could contribute to an increase the RRRV [27, 30, 31].

Table 20: TRV peak for case scenario 1-6.

Case scenario	**TRV peak 1. pole to clear [kV]**	**TRV peak 2. pole to clear [kV]**	**TRV peak 3. pole to clear [kV]**
1: Line 0.6 km	13.78	10.15	9.56
2: Line 0.8 km	13.74	9.99	9.59
3: Line 1 km	13.89	10.13	9.72
4: Line 2 km (base case)	14.79	11.75	10.92
5: Line 3 km	15.52	13.11	11.94
6: Line 5 km	18.73	15.94	12.57

The TRV peak results for case scenario 1-6 are shown in Table 20. The T60 capability curve is used for the 0.6 km and the 0.8 km lines, while the T30 capability curve is used for all the other chosen line lengths. The highest peak is measured to 18.73 kV, and it is measured in the first pole to clear for a line of 5 km. The lowest peak is observed in the third pole to clear for a line length of 0.6 km. None of the values in Table 20 exceeds the capability of the breaker which is 48.4 kV for T60 and 51.2 kV for T30.

The trend that can be observed in Table 20 is that the highest TRV peak for each of the line lengths is observed in the first pole to clear. This observation

is expected due to the shift in neutral point caused by the high impedance between neutral and ground in the induction machine used in the DFIG.

In addition, the TRV peak is increasing with an increasing line length for all the poles to clear. This observation is valid for all the line lengths from 0.8-5 km.

4.2.3 Case Scenario 7-12. Changing the Overhead Line (*TLine_1*) to an Underground Cable (*Cable_1*)

Table 21: RRRV for case scenario 7-12.

Case scenario	**RRRV 1. pole to clear [kV/μs]**	**RRRV 2. pole to clear [kV/μs]**	**RRRV 3. pole to clear [kV/μs]**
7: Cable 0.6 km	2.479	1.996	1.695
8: Cable 0.8 km	2.704	2.207	1.508
9: Cable 1 km	2.689	2.091	1.584
10: Cable 2 km	2.671	2.072	1.561
11: Cable 3 km	2.485	1.922	1.611
12: Cable 5 km	2.263	1.850	1.413

In Table 21 the RRRVs for the first, second and third pole to clear for case scenario 7-12 are presented. The fault current for cables with a length of 0.6 km, 0.8 km and 1 km is between 30 % and 60 % of the breaking capacity, so the T60 capability curves are used for these cable lengths. For all the other chosen cable lengths the T30 capability curves are used. The steepness of the T60 capability curve is 1.16 kV/μs while the steepness of the T30 curve is 2.47 kV/μs as shown in Table 2 in Section 2.3.

The values marked with red are the RRRVs that exceed the relevant capability curve for a S1 circuit breaker rated 24 kV. As opposed to case scenario 7-11, the RRRVs for all the three poles to clear are within the capability of the breaker in case scenario 12 for a cable of 5 km. The steepest RRRV is observed in the first pole to clear for a cable of 0.8 km, and is measured to 2.704 kV/μs. The lowest RRRV is observed in the third pole to clear for a cable of 5 km and is measured to 1.413 kV/μs.

By comparing the RRRVs observed in the wind power network for case sce-

nario 1-6 to the RRRVs observed in case scenario 7-12 some observations can be made. One similarity is that for the five shortest line/cable lengths the RRRV exceeds the capability of the breaker. In addition, the longest chosen line/cable length of 5 km results in a situation where the breaker is operating within its capability. It can also be noticed that in the line case the steepest RRRV is found for a line of 0.6 km, while the steepest RRRV in the cable case is observed for a cable of 0.8 km. This observation is reasonable as cables and lines can have different critical lengths.

Table 22: TRV peak for case scenario 7-12.

Case scenario	**TRV peak 1. pole to clear [kV]**	**TRV peak 2. pole to clear [kV]**	**TRV peak 3. pole to clear [kV]**
7: Cable 0.6 km	13.08	9.35	9.82
8: Cable 0.8 km	13.11	9.40	10.00
9: Cable 1 km	13.14	9.44	10.13
10: Cable 2 km	13.26	9.61	10.53
11: Cable 3 km	13.39	9.72	10.76
12: Cable 5 km	13.70	10.04	11.08

The TRV peak values for the first, second and third pole to clear are presented in Table 22. The T60 curve is used for cables with lengths of 0.6 km, 0.8 km and 1 km, while the T30 curve is used for all the other cable lengths. The T30 capability curve of an S1 circuit breaker rated 24 kV has a peak value of 47.0 kV while the T60 capability curve has a peak of 44.1 kV as shown in Table 1 in Section 2.3. All of the values presented in Table 22 is within the capability of the breaker. The highest TRV peak is observed in the first pole to clear for a cable of 5 km, and is measured to 13.70 kV. The lowest TRV peak is seen in the second pole to clear for a cable of 0.6 km, and is measured to 9.35 kV.

The trend that can be observed in Table 22 is that the highest TRV peak for each cable length is measured in the first pole to clear. In addition, in Table 22 it can be seen that increasing the cable length leads to an increase in the TRV peak.

4.2.4 Case Scenario 13-16. Changing the Power Flowing through the Breaker

Table 23: RRRV for case scenario 13-16.

Case scenario	RRRV 1. pole to clear [kV/μs]	RRRV 2. pole to clear [kV/μs]	RRRV 3. pole to clear [kV/μs]
13: 5 MW flowing through the breaker	1.398	1.029	1.115
14: 9 MW flowing through the breaker	1.969	1.464	1.436
15: 13 MW flowing through the breaker	2.473	1.722	1.514
16: 20 MW flowing through the breaker (base case)	3.086	2.291	1.758

In Table 23 the RRRVs for the first, second and third pole to clear for case scenario 13-16 are presented. In case scenario 13 the peak of the fault current is below 10 % of the breaking capacity, so the T10 capability curves are used in this case scenario. For case scenario 14-16 the peak of the fault current is between 10 % and 30 % of the breaking capacity, so the T30 capability curves are used in these scenarios.

The capability of the breaker is only exceeded in the first pole to clear for 20 MW flowing through the breaker. In this case the RRRV is measured to 3.086 kV/μs, which is higher than the T30 capability curve of 3.01 kV/μs. The lowest RRRV is measured to 1.029 kV/μs in the second pole to clear for a power flow of of 5 MW.

By investigating Table 23 it can be noticed that the steepness of the RRRV is increasing with an increased power flow. The same trend is also observed in the photovoltaic network as presented in Table 15. An increased power flow results in an increased short circuit current. This means that increasing

the short circuit current could contribute to an increased RRRV. This observation is also found in the study presented in [27]. Another observation concerning the RRRVs in Table 23 is that the steepest RRRV for all the chosen power flows is observed in the first pole to clear.

Table 24: TRV peak for case scenario 13-16.

Case scenario	**TRV peak 1. pole to clear [kV]**	**TRV peak 2. pole to clear [kV]**	**TRV peak 3. pole to clear [kV]**
13: 5 MW flowing through the breaker	12.05	7.83	9.30
14: 9 MW flowing through the breaker	12.80	8.89	9.66
15: 13 MW flowing through the breaker	13.50	9.85	10.01
16: 20 MW flowing through the breaker (base case)	14.79	11.75	10.92

In Table 24 the TRV peak values for the first, second and third pole to clear are shown. The highest peak is observed in the first pole to clear for a power flow of 20 MW, and it is measured to 14.79 kV. The lowest TRV peak is observed for a power flow of 5 MW in the second pole to clear, and is measured to 7.83 kV.

In similarity to case scenario 1-12 performed on the wind power network, the highest TRV peaks are observed in the first pole to clear. As explained earlier, the reason behind this is the shift in neutral point.

Another trend observed in Table 24 is that increasing the power flow within the chosen range results in an increase in the TRV peak.

4.2.5 Case Scenario 17-20. Changing the Time between the Short Circuit Instant and the Breaker Contacts Separation.

Table 25: RRRV for case scenario 17-20.

Case scenario	RRRV 1. pole to clear [kV/μs]	RRRV 2. pole to clear [kV/μs]	RRRV 3. pole to clear [kV/μs]
17: 43 ms between short circuit and contact separation (base case)	3.086	2.291	1.758
18: 63 ms between short circuit and contact separation	1.360	0.746	1.288
19: 83 ms between short circuit and contact separation	2.505	2.343	2.046
20: 103 ms between short circuit and contact separation	3.043	3.081	2.191

The RRRVs for the first, second and third pole to clear for case scenario 17-20 are presented in Table 25. The T30 curve of 3.01 kV/μs is the relevant capability curve for all the scenarios presented in Table 25. The capability of the breaker is exceeded for the shortest and the longest time instants between the fault and the contact separation. In case scenario 20 the RRRV actually exceeds the capability of the breaker both in the first and second pole to clear. The steepest RRRV is measured for case scenario 17, and is measured to 3.086 kV/μs. The lowest RRRV is measured in the second pole to clear in case scenario 18, and is measured to 0.746 kV/μs.

The trend observed in Table 25 is that the steepest RRRVs are observed for the shortest and the longest chosen time instants. To make sure that this observation was not a coincidence, it was decided to investigate the time between the short circuit and the contact separation further. The following time instants were then investigated: 40, 44, 45, 46, 47, 48, 49, 50, 55, 60, 65, 80, 85, 90, 93, 94, 95, and 100 ms. The result showed a range were the capability of the breaker is not violated. This range is between 46-93 ms,

while the values under and above this range resulted in a violation of the capability of the breaker. The explanation to why this range is observed could be related to the fault current. By investigating the fault current further is was observed that the peak of the fault current was smallest in the interval between 46-93 ms. As mentioned earlier, an increase in the current could contribute to an increase in the RRRV [27, 30, 31].

Table 26: TRV peak for case scenario 17-20.

Case scenario	**TRV peak 1. pole to clear [kV]**	**TRV peak 2. pole to clear [kV]**	**TRV peak 3. pole to clear [kV]**
17: 43 ms between short circuit and contact separation (base case)	14.79	11.75	10.92
18: 63 ms between short circuit and contact separation	5.41	6.19	8.15
19: 83 ms between short circuit and contact separation	15.10	17.42	16.97
20: 103 ms between short circuit and contact separation	19.20	20.97	18.54

The TRV peak values for the first, second and third pole to clear for case scenario 17-20 are presented in Table 26. The peak of the T30 capability curve of 51.2 kV is used in case scenario 17-20. None of the values in Table 26 exceeds the relevant capability curve. The highest TRV peak is observed in the second pole to clear in case scenario 20, and is measured to 20.97 kV. The lowest TRV peak is measured to 5.41 kV, and it is observed in the first pole to clear for 63 ms between the fault instant and the contact separation.

4.3 Comparison of the Resulting TRV from the Wind Network and the PV Network

Some interesting observations can be made by comparing the resulting TRV from case scenario 1-20 of the wind power network and the PV network. The RRRVs observed in both of the networks will be compared first. Secondly,

the TRV peak values will be compared.

By comparing the results from case scenario 1-6 it can be noticed that in both the PV and the wind network the steepest RRRV is measured for a line length of 0.6 km. In the PV network the steepest RRRV is measured to 0.658 kV/μs, while in the wind power network the steepest RRRV is measured to 3.167 kV/μs. In general the RRRVs are steeper for the shortest line lengths in both the wind and the PV network. The reason behind this is probably because the fault current increases when the line length is decreasing. Increasing the current could result in an increase the RRRV [27, 30, 31]. Another important observation is that in the PV network the breaker is operating within its limit for all the chosen line lengths, while in the wind network the breaker is operating within its capability only for a line length of 5 km.

Regarding the results of case scenario 7-12 it can be observed that the steepest RRRV in the PV network is observed for a cable of 0.6 km, while the steepest RRRV in the wind network is observed for a cable of 0.8 km. The steepest RRRV is measured to 0.508 kV/μs in the PV network, while the steepest RRRV in the wind network is measured to 2.704 kV/μs. The lowest RRRVs are in general seen in the longest cable lengths. The explanation to this is probably the increased current for the shorter cable lengths. Concerning the breaker capability, in the PV network the breaker is operating within its capability for all the chosen cable lengths, while in the wind network the capability of the breaker is exceeded for the five shortest chosen cable lengths.

Concerning the results of case scenario 13-16 it can be noticed that the steepest RRRV is observed for a power flow of 20 MW through the breaker in both the PV and the wind network. In the PV network the steepest RRRV is measured to 0.574 kV/μs, while the steepest RRRV in the wind network is measured to 3.086 kV/μs. The RRRVs are in general higher for larger power flows in both the PV and the wind network. This is probably because the fault current is higher for larger amounts of power flow which can increase the RRRVs [27, 30, 31]. Regarding the capability of the breaker, in the wind power network only the largest power flow of 20 MW results in a situation where the capability of the breaker is exceeded. In the PV network the breaker is operating within its limit for all the chosen amounts of power flow.

By comparing the results of case scenario 17-20 it can be observed that the steepest RRRV in the PV network is observed in case scenario 20, while

the steepest RRRV in the wind network is observed in case scenario 17. The steepest RRRV in the PV network is 0.652 kV/μs, while the steepest RRRV in the wind network is measured to 3.086 kV/μs. In the wind power network it was observed that the RRRVs were higher for the time instants corresponding to a higher peak of the fault current. The breaker is operating beyond its capability in the wind power network in both case scenario 17 and 20. In the PV network the breaker is operating within its capability for all the chosen time instants between the fault and the contact separation.

Concerning the TRV peak values, both the PV and the wind network are operating within the capability of the breaker in all the case scenarios (1-20). In the wind power network the highest TRV peaks were in general observed in the first pole to clear. This observation is probably caused by a shift in the neutral due to the resistance of 1000 Ω connected between neutral and ground in the induction generator used in the DFIG. However, this observation was not valid for the three longest chosen time instants between the fault and the contact separation.

On the other hand, in the PV network the highest TRV peaks were not observed in the first pole to clear but in the second or third pole to clear. The reason behind this difference between the wind and the PV network could be because there is no impedance as high as 1000 Ω connected between neutral and ground in the PV network. Even though a dependency between the phases is observed in the PV network (due to the coupling between the conductors in the line/cable), the dependency will not result in a shift in the neutral point. The coupling between the conductors is the dominating effect in the PV network which result in a higher TRV peak for the second and third pole to clear compared to the first pole to clear.

4.4 Source of Errors

- The RRRV values presented in this chapter had to be calculated by hand. It was observed some deviation in the calculated RRRV dependent on which two points on the curve that were used in the RRRV calculation. This deviation is in the range of 5 %. This possible source of error could change which of the case scenarios that resulted in the worst RRRV, but it will not change the main conclusions drawn in this study. As mentioned in the modeling chapter, the violations of the capability curve were observed with the use of the *TRV Envelope Component*, and could not have been affected by the manual calculation of the RRRVs.

- As mentioned in the modeling section, a current chopping limit of 0 kA was chosen. In reality, this chopping limit is not correct in the case of vacuum interrupters. In vacuum breakers the current can be chopped for values in the range of 3.5-25 A, dependent on the material of the contacts [2].

- In all the simulations performed in this thesis the arc voltage is neglected. In real life it would contribute to reduce the TRV to some extent. The arc voltage of vacuum breakers and medium voltage SF_6 breakers are assumed to be *Low* (≤ 1 kV) [2]. Including the arc voltage will probably decrease the TRV peak to some extent, but it is difficult to say whether or not this will contribute to reduce the RRRVs.

- The PSCAD simulation tool could be a source of error itself if for example some numerical peaks are misinterpreted as a valid simulation result.

5 Conclusion

Transient models of a grid connected wind power network and a grid connected photovoltaic network have been made in this thesis. These models have then been used to examine the transient recovery voltage resulting from a short line fault in networks with distributed generation. The effect of changing four different parameters were studied with the use of 20 case scenarios.

In the photovoltaic network it was observed that both the TRV peak and the RRRV were kept inside the capability of the breaker for all the chosen parameter variations. Among all the case scenarios, the highest RRRV observed in the PV network was observed in the scenario with a line of 0.6 km. This RRRV was measured to 0.658 kV/μs, and it is within the relevant capability curve of the breaker which is the T30 curve of 3.01 kV/μs.

On the other hand, in the wind power network there were observed several parameter variations that resulted in a violation of the capability of the breaker. In similarity to the PV network, the highest RRRV measured in the wind power network was observed in the case scenario with a line of 0.6 km. This RRRV was measured to 3.167 kV/μs, and it is exceeding the relevant capability of the breaker which is the T60 curve of 1.67 kV/μs. The RRRV exceeded the breaker capability for a cable/line with lengths between 0.6-3 km. In addition, the breaker was operating beyond its limit in the case scenarios with 43 ms and 103 ms between the short circuit instant and the contact separation. By comparing the RRRVs for different power flows through the breaker it was observed that only the highest power flow of 20 MW resulted in a violation of the breaker capability.

Regarding the TRV peak values in the wind power network, it was observed that the peak TRV was kept inside the capability of the breaker for all the chosen case scenarios.

In both the wind power network and the photovoltaic network it was observed that the RRRV was increasing with an increased fault current. The explanation to why the steepest RRRVs observed in this study were seen in the wind power network could be related to the high fault currents observed in the wind power network compared to the photovoltaic network.

The high RRRVs observed in the wind power network can be mitigated by adding capacitors to the circuit breaker terminal(s), to a bus or to a line/cable [22, 31]. Another option is to replace the circuit breaker itself by

a circuit breaker with a higher voltage and/or current rating [22].

It should be mentioned that this study only investigates whether or not the TRV peak and the RRRV exceeds the capability of the breaker. This means that other parameters related to the capability of the breaker that are not in the scope of this study could have been violated. One example of these parameters is the arcing time.

Finally, it is essential to add that all the values presented in the result chapter is only valid for the given network configurations and can not be seen as general for all distribution networks with photovoltaic or wind power connected. The high RRRVs observed in the wind power network is an interesting finding and should be investigated further. However, the high RRRVs in the wind network should not be interpreted as a general rule as the transient recovery voltage is highly dependent on the network parameters.

5.1 Recommendations for Further Work

- Parameters from a real network can be implemented in the network models, and the same simulations can be performed again.
- The effect of changing four different network parameters were investigated in this thesis. In future studies other parameters should be investigates as well, such as:
  - Different fault types: line-to-line, single line-to-ground, three line-to-ground, and three line.
  - Different fault locations: terminal of the breaker, the terminal of the generating unit, a distance away from the breaker, and etc.
  - Since the resulting TRV from the PV network and the wind power network was to be compared in this thesis, the scaling component were used in both of the networks. In a future study it would be possible to do this investigation without the scaling component in the PV network. In this way it would be necessary to change the parameters of the LCL-filter and the transformer MVA when the output power from the PV plant is changed. This would make it possible to observe the effect of changing the LCL- filter, the transformer MVA, and the power flow, and not only the effect of changing the power flow which is studied in this thesis.

6 Bibliography

[1] S. K. Wetjen. *Investigation of Stresses on Switching Devices in Networks With Distributed Energy Resources*. December 2018.

[2] K. Niayesh and M. Runde. *Power Switching Components: Theory, Applications and Future Trends*. 1st. Springer, 2017.

[3] H. Sæle. *Distributed Generation and Prosumers*. Website. last checked: 04.04.2019. URL: https://www.sintef.no/en/distributed%5C-production/.

[4] G. Pepermans, J. Driesen, D. Haeseldonckx, R. Belmans, and W. D'haeseleer. "Distributed Generation: Definition, Benefits and Issues". In: *Energy policy* 33.6 (2005), pp. 787–798.

[5] N. Nimpitiwan, G. T. Heydt, J. Blevins, and A. B. Cummings. "Potential Economic Impact of Fault Currents Contributed by Distributed Generation". In: *IEEE Power Engineering Society General Meeting* (2005), p. 1.

[6] S. Kotamarty, S. Khushalani, and N. Schulz. "Impact of Distributed Generation on Distribution Contingency Analysis". In: *Electric Power Systems Research* 78.9 (2008), pp. 1537–1545.

[7] S. Ahmad, S. Sardar, A. U. Asar, and B. Noor. "Impact of Distributed Generation on the Reliability of Local Distribution System". In: *International Journal of Advanced Computer Science and Applications* 8.6 (2017), pp. 375–382.

[8] Electrical Engineering Design Services. *Generating, Transmitting, and Distributing Electricity*. Website. last checked: 29.11.2018. URL: http://electricalengineeringdesignservices.blogspot.com/2012/02/generating-transmitting-and.html.

[9] G. M. Masters. *Renewable and Efficient Electric Power Systems*. John Wiley & Sons, 2013.

[10] N. Mohan and W. P. Robbins. *Power Electronics: Converters, Applications, and Design*. Wiley, 2002.

[11] ABB. "Technical Application Papers No.10. Photovoltaic plants". In: (2010).

[12] H. I. Cho, S. M. Yeo, C. H. Kim, W. Terzija, and Z. M. Radojevic. "A steady-state model of the Photovoltaic System in EMTP". In: *International Conference on Power Systems Transients (IPST2009).* 2009, pp. 3–6.

[13] A. Rajapakse. *Simulation of Grid Connected Photovoltaic Systems.* Website. last checked: 10.11.2018. URL: https://hvdc.ca/uploads/knowledge_base/pv_article.pdf?t=1467109305.

[14] A. Kumar, N. Gupta, and V. Gupta. "A Comprehensive Review on Grid-Tied Solar Photovoltaic System". In: *Journal of Green Engineering* 7.1 (2017), pp. 213–254.

[15] D. F. Howard. "Short-Circuit Currents in Wind-Turbine Generator Networks". In: (2013), p. 273.

[16] H. Saadat. *Power System Analysis.* PSA Publishing, 2010.

[17] M. A. Abdullah, A. H. M. Yatim, C. W. Tan, and R. Saidur. "A Review of Maximum Power Point Tracking Algorithms for Wind Energy Systems". In: *Renewable and Sustainable Energy Reviews* 16.5 (2012), pp. 3220–3227.

[18] N. Mourad and B. Mohamed. "Short Circuit Current Contribution of Distributed Photovoltaic Integration on Radial Distribution Networks". In: *Electrical Engineering (ICEE), 2015 4th International Conference on.* IEEE. 2015, pp. 1–4.

[19] R. J. Bravo and C. Ly. "Electronic-Coupled Generators Short Circuit Impacts". In: *Seventh Annual IEEE Green Technologies Conference* (2015), p. 4.

[20] J. Machowski, J. W. Bialek, and J. R. Bumby. *Power System Dynamics and Stability.* John Wiley & Sons, 1997.

[21] R. Rifaat, T. S. Lally, and J. Hong. "Circuit Breaker Transient Recovery Voltage Requirements for Medium-Voltage Systems With NRG". In: *IEEE Transactions on Industry Applications, VOL. 50, NO. 5,* (2014), p. 7.

[22] IEEE C37.011. "IEEE Guide for the Application of Transient Recovery Voltage for AC High-Voltage Circuit Breakers". In: (2011).

[23] IEEE C37.06. “IEEE Standard for AC High-Voltage Circuit Breakers Rated on a Symmetrical Current Basis - Preferred Ratings and Related Required Capabilities for Voltages Above 1000 V”. In: (2009).

[24] IEC 62271-100. “High-Voltage Switchgear and Controlgear–Part 100: Alternating Current Circuit-Breakers”. In: (2011).

[25] S. N. Afifi, H. Wang, G. A. Taylor, and M. R. Irving. “Impact of DFIG Wind Turbines on Short Circuit Levels in Distribution Networks using ETAP”. In: *Power Engineering Conference (UPEC), 2013 48th International Universities'*. IEEE. 2013, pp. 1–4.

[26] B. Badrzadeh. “Transient Recovery Voltages Caused by Capacitor Switching in Wind Power Plants”. In: *IEEE Transactions on Industry Applications* 49.6 (2013), pp. 2810–2819.

[27] Z. Zhou, X. Wang, and P. Wilson. “Transient Recovery Voltage Assessment for 138kv Breakers with the New Addition of a Wind Farm”. In: *Power System Technology, 2006. PowerCon 2006. International Conference on*. IEEE. 2006, pp. 1–5.

[28] Manitoba HVDC Research Senter. *Transient Recovery Voltage (TRV) Study*. Website. last checked: 26.03.2019. URL: https://hvdc.ca/uploads/knowledge_base/breaker_trv_studies.pdf?t=1466194850.

[29] H. K. Høidalen. *TET 4130 Overspenninger og Overspenningsvern*. 2007.

[30] R. Smeets, L. Sluis, M. Kapetanovic, D. F. Peelo, and A. Janssen. *Switching in Electrical Transmission and Distribution systems*. John Wiley & Sons, 2014.

[31] D.F. Peelo. *Current interruption transients calculation*. Wiley, 2014.

[32] IEC 62271-1. “High Voltage Switchgear and Controlgear Part 1: Common Specifications for Alternating Current Switchgear and Controlgear”. In: (2017).

[33] NEK 450-2. “NEK Electrotechnical Terminology”. In: (2002).

[34] ABB. *VD4 Medium Voltage Vacuum Circuit-Breakers with Modular Operating Mechanism*. Website. last checked: 07.03.2019. URL: https://library.e.abb.com/public/aabb75731fcc41a281211a111489abb3/2017.11.22%5C%20%5C%20VD4%5C%2012kV%5C%20Brochure%5C%20.pdf.

[35] ABB. *VM1 Vacuum Circuit-Breakers with Magnetic Acutator Mechanism*. Website. last checked: 07.03.2019. URL: https://library.e.abb.com/public/81408d8d5ba2ff9cc1257b4a0047a8f6/2491%5C%20Flyer%5C%20VM1%5C%20GB.pdf?x-sign=nCymKEt6RPn2FLsMVyB11bpgqktu62mAvBnT1tNBE2bkDBv9OTWz0EF+DZn1vfv5.

[36] ABB. *HD4 Gas insulated MV circuit Breakers up to: 40.5 kV; 4000 A; 50 kA*. Website. last checked: 07.03.2019. URL: https://library.e.abb.com/public/5352e698931f41ae966a3582fc55135a/CA_HD4(EN)T_1VCP000004_06.2018.pdf?x-sign=Mr/0Ltimm2IaMZiPisWrsbAI68MqFe3xytd/B2VBBghjhLebzsj43mykEl4Dhyii.

[37] IEC 60077-4. "Railway Applications - Electric Equipment for Rolling Stock Part 4: Electrotechnical Components- Rules for AC Circuit Breakers". In: (2003).

[38] PSCAD. *User's Guide on the Use of PSCAD*. Website. last checked: 22.02.2019. URL: https://hvdc.ca/uploads/knowledge_base/pscad_manual_v4_6.pdf?t=1528395602.

[39] PSCAD. *Knowledge Base*. Website. last checked: 22.11.2018. URL: https://hvdc.ca/knowledge-base/v:.

[40] Manitoba HVDC Research Senter. *Webinar on Transient Recovery Voltage TRV Simulations in PSCAD^{TM} EMTDC^{TM}*. Website. last checked: 28.11.2018. URL: https://www.youtube.com/watch?v=LYqPSeIYcL8.

[41] PSCAD. *Type 3 Wind Turbine Model*. Website. last checked: 10.11.2018. Revision 2. URL: https://hvdc.ca/uploads/knowledge_base/type_3_wind_turbine_model.pdf?t=1542818424.

[42] T. Kuczek, M. Florkowski, and W. Piasecki. "Analyses of Vacuum Circuit Breaker Switching Transients in Medium Voltage Networks with respect to LC Filters of Solar Converters".

In: *2014 ICHVE International Conference on High Voltage Engineering and Application*. IEEE. 2014, pp. 1–4.

7 Abbreviations

DFIG Doubly Fed Induction Generator

DG Distributed Generation

EMTDC Electromagnetic Transient Simulation Engine

GSC Grid Side Converter

MPP Maximum Power Point

MPPT Maximum Power Point Tracker

PLL Phase Locked Loop

PSCAD Power Systems Computer Aided Design

PV Photovoltaic

RRRV Rate of Rise of Recovery Voltage

RSC Rotor Side Converter

SCL Short Circuit Level

SG Synchronous Generator

THD Total Harmonic Distortion

TRV Transient Recovery Voltage

VSC Voltage Source Converter

WTG Wind Turbine Generator

WRIG Wound Rotor Induction Generator

A Appendices

A.1 Appendix I - Steady State Results

The steady state results are divided into two sections: *Photovoltaic Base Case Network* and *Wind Power Base Case Network*. The waveforms of voltage, current, real power, and reactive power are shown for each of the systems.

Photovoltaic Base Case Network
All the parameters shown in this section corresponds to the names above the multimeters shown in Figure 15 and Figure 16 presented in Section 3.2.1.

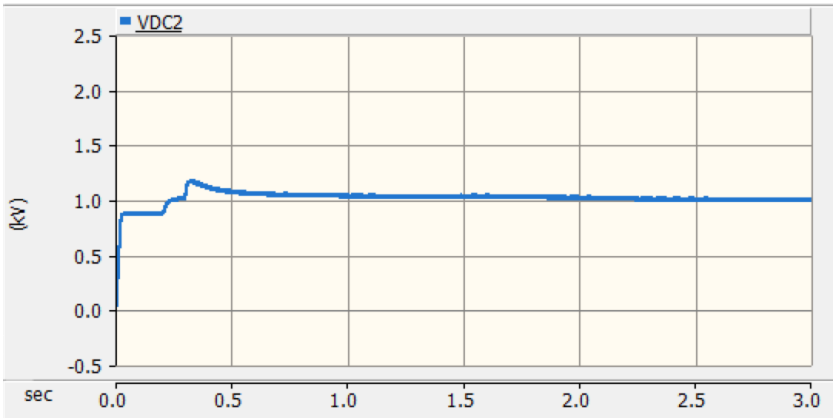

Figure 44: DC voltage input to VSC.

The input voltage to the voltage source controller named *VDC2* is presented in Figure 44. It can be observed that the set-value of 1 kV is kept from 1 sec to 3 sec.

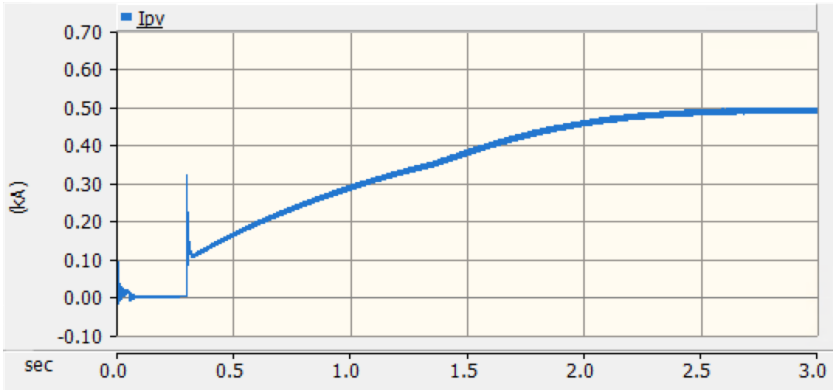

Figure 45: Output DC current from PV array.

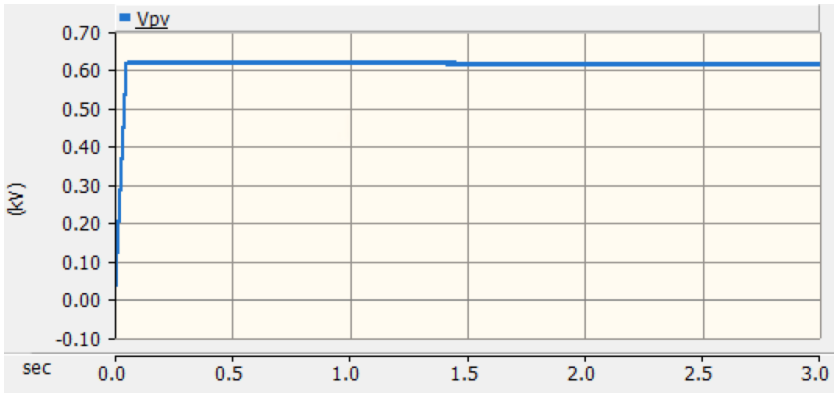

Figure 46: Output DC voltage from PV array.

The DC current and voltage output from the PV array is presented in Figure 45 and Figure 46, respectively. It can be observed that the current is kept at 0.5 kA from 2.5-3 sec, while the voltage is kept at 0.62 kV from 1.5-3 sec.

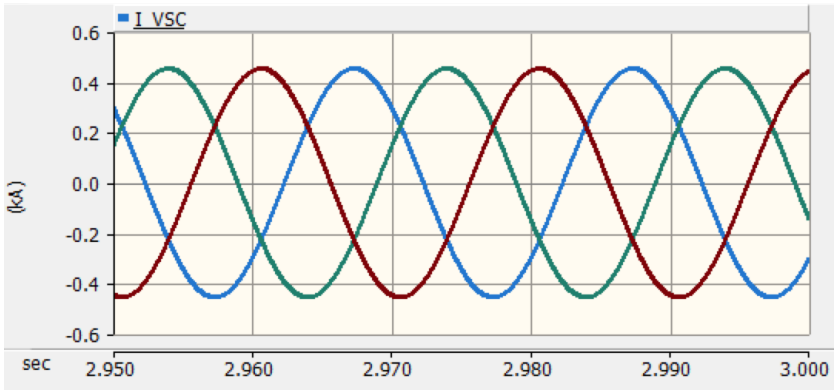

Figure 47: Output AC current from PV system.

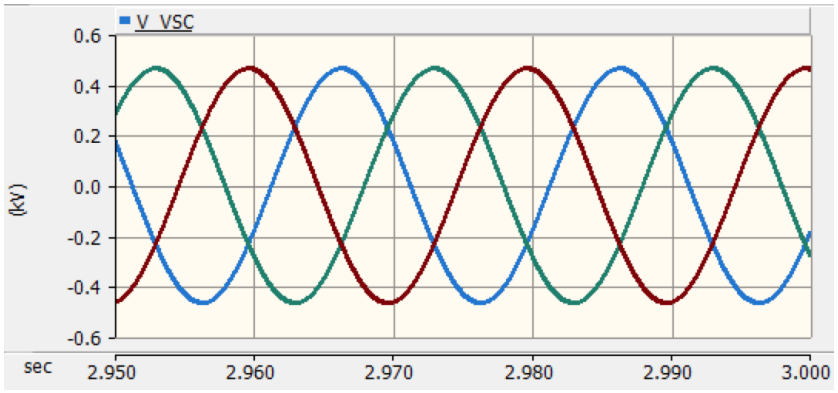

Figure 48: Output AC phase voltage from PV system.

In Figure 47 and Figure 48 the AC output current and voltage from the voltage source converter is shown. It can be obseved that the peak value of the current is 0.43 kA while the peak value of the output voltage is $0.6 * \frac{\sqrt{2}}{\sqrt{3}} = 0.49$ kV line to ground. In addition, it can be seen that the frequency is 50 Hz in both the voltage and current, and there are not any distinct harmonics present.

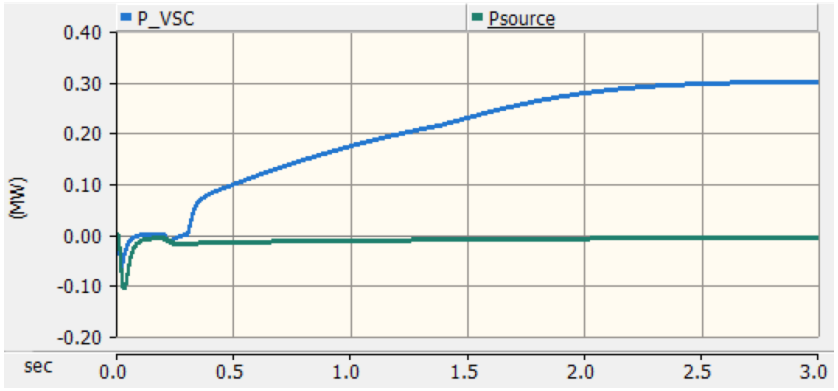

Figure 49: Real power generated by the PV system (blue) and real power generated by the source (green).

The real power generated by the PV system and the source is presented in Figure 49. It can be observed that the real power generated by the PV system is 0.3 MW while the real power generated by the source is close to zero. Both the power from the PV system and the source has stabilized before 3 sec.

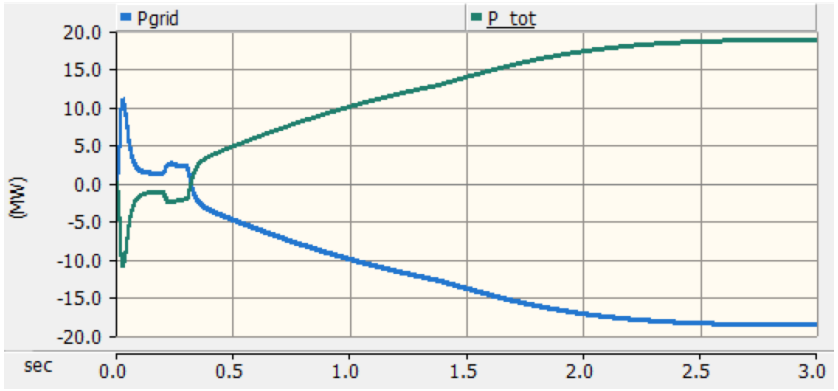

Figure 50: Total real power generated (green) and real power generated by the distribution grid equivalent (blue).

In Figure 50 the total real power generated by the grid and generated by the distribution grid equivalent is shown. Around 19.72 MW is generated in total by all the PV plants connected in parallel, while 18.87 MW is consumed by the distribution grid equivalent. The difference in generated and consumed power is caused by the power loss in the overhead lines.

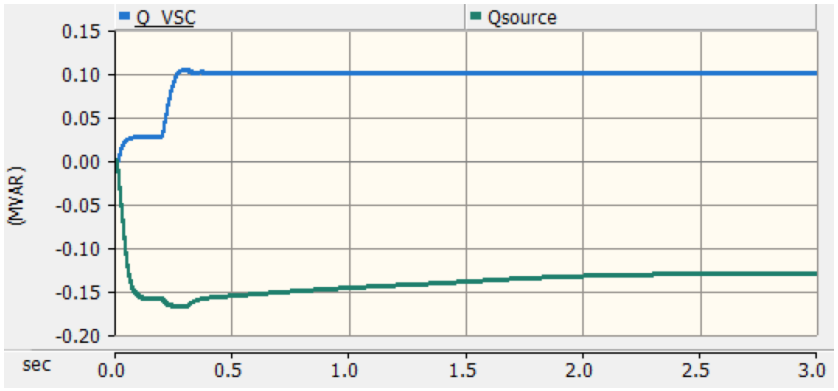

Figure 51: Reactive power generated by the VSC (blue) and source (green).

The reactive power generated by the voltage source converter and the source is shown in Figure 51. Both of the values are stabilized within 3 sec.

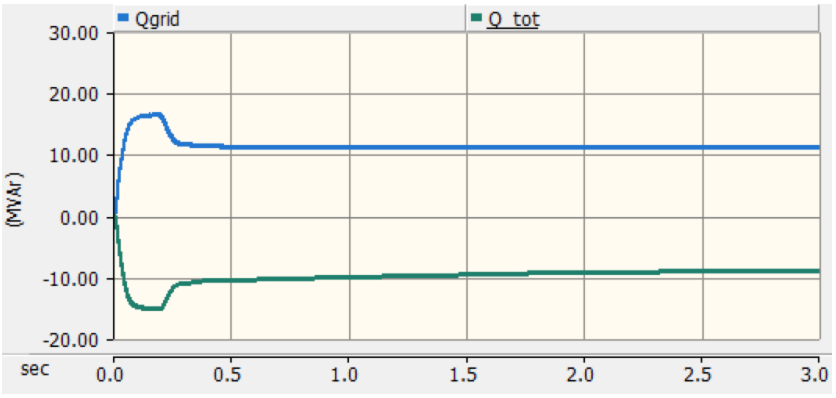

Figure 52: Reactive power generated by the distribution grid (blue) and total reactive power generated by the PV plant(green).

In Figure 52 the reactive power generated by the distribution grid and the total reactive power generated by the PV plant is presented. Both of the values are stabilized within 3 sec. The difference between these two are reactive power consumed in the overhead lines.

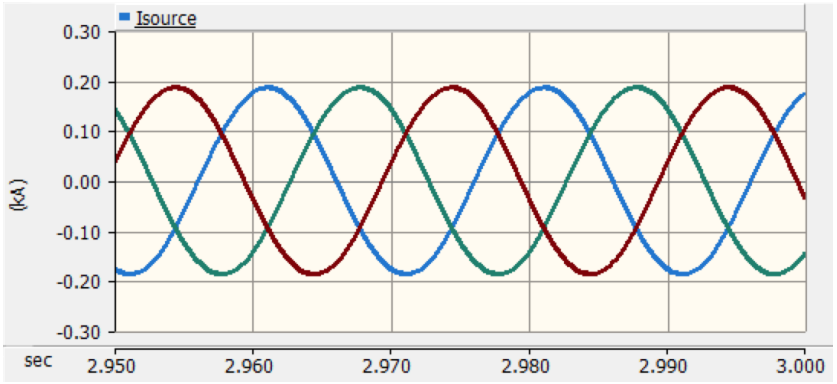

Figure 53: Output current from the source.

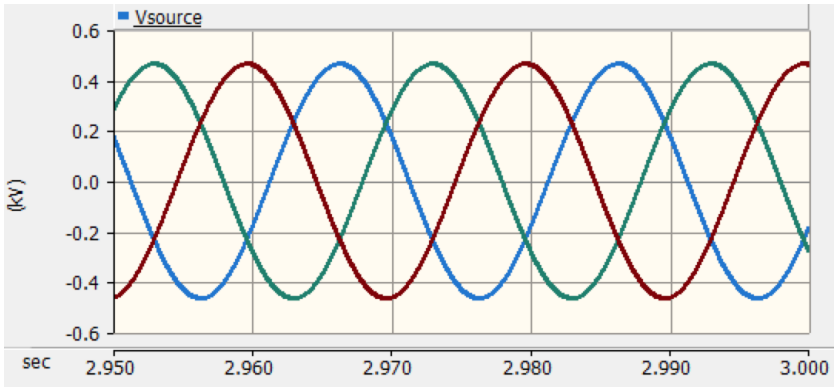

Figure 54: Output voltage from the source.

In Figure 53 and Figure 54 the output current and voltage from the source is presented. It can be observed that the peak of the voltage is 0.49 kV line to ground while the peak of the current is around 0.2 kA. By comparing the output current from the source to the output current from the VSC it can be observed that the output current from the source is around half the output current from the VSC. The output voltage from the source is equal to the output voltage from the VSC as expected.

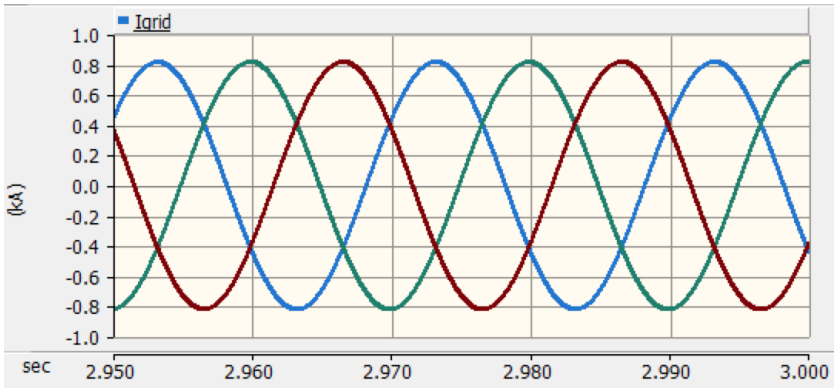

Figure 55: Current flowing into the distribution grid equivalent.

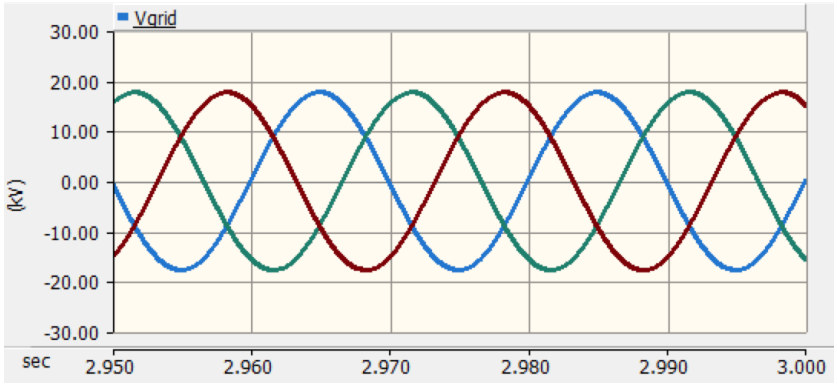

Figure 56: Voltage at the distribution grid equivalent.

In Figure 55 and Figure 56 the current and the voltage measured at the terminal of the distribution grid equivalent is presented. The peak value of this current is around 0.81 kA. The peak phase voltage is measured to 17.70 kV. This peak phase voltage corresponds to a line to line RMS voltage of $17.70 * \frac{\sqrt{3}}{\sqrt{2}} = 21.68$ kV, which is within the margin of 7 %.

Wind Power Base Case Network

All the parameters shown in this section corresponds to the names above the multimeters shown in Figure 18 and Figure 19 presented in Section 3.2.2.

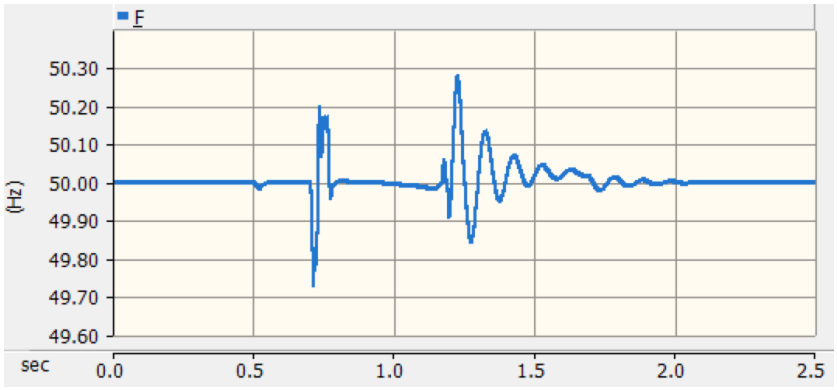

Figure 57: Frequency in the network.

In Figure 57 the frequency in the wind power network is presented. It can be observed that it deviates from 50 Hz in some periods, but it is kept stable at 50 Hz from 2 sec. The reason behind this deviations in the frequency is the time instants when the wind turbines are connected to the rest of the network.

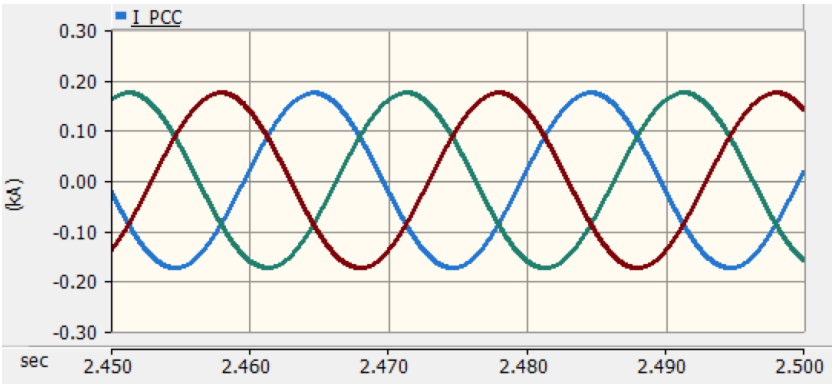

Figure 58: Output current from one wind turbine.

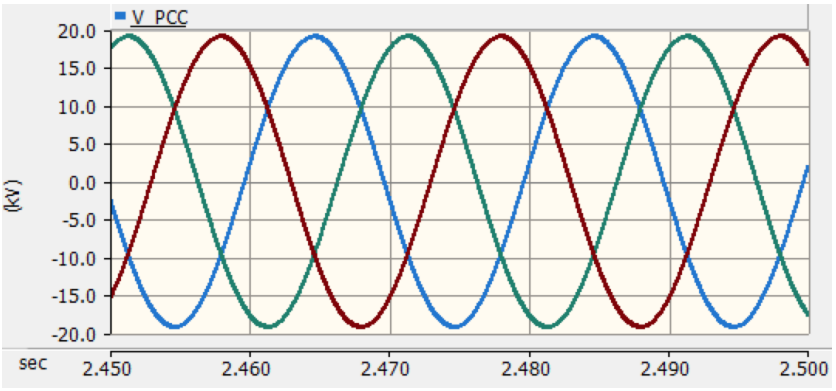

Figure 59: Voltage at the WindBus.

In Figure 58 and Figure 59 the output current from one wind turbine and the voltage at the WindBus are shown. It can be observed that the current has a peak value of 0.17 kA, while the peak value of the voltage is 19.14 kV line to ground. The voltage is inside the margin of 7 %, and the resulting line to line RMS voltage can be found: $19.14 * \frac{\sqrt{3}}{\sqrt{2}} = 23.44$ kV.

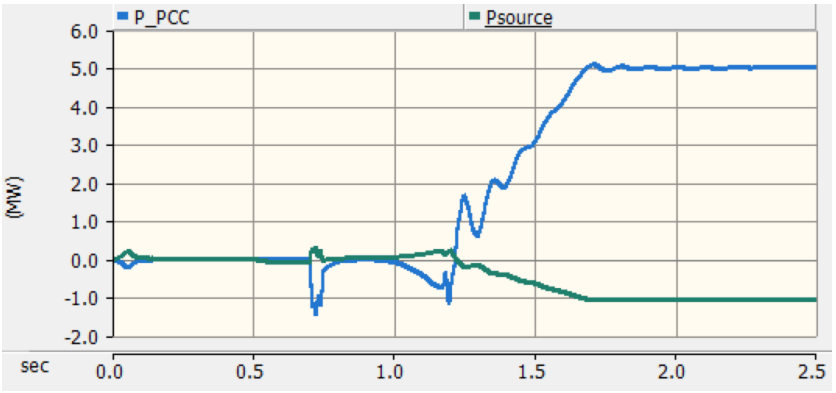

Figure 60: Real power generated by one wind turbine (blue) and real power generated by the source (green).

In Figure 60 the real power generated by one wind turbine and by the source is presented. The real power generated by one wind turbine is 5.00 MW, and is equal to the rated power of one wind turbine. The real power consumed by the source is 1.06 MW. The real power generated by one wind turbine and by the source has both reached steady state at 2.3 sec.

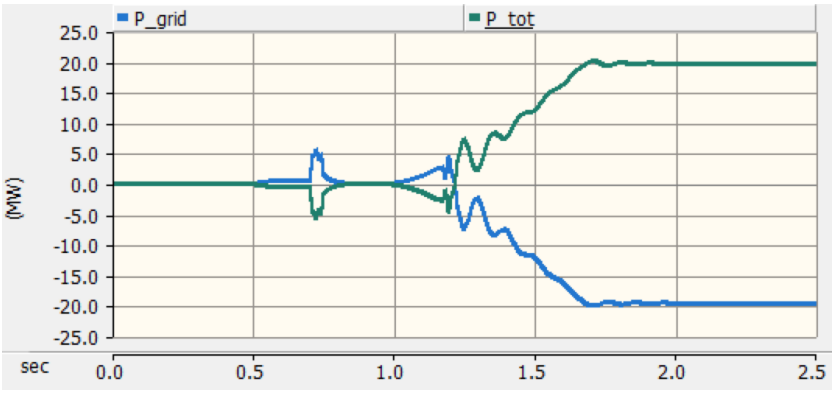

Figure 61: Total real power generated by the wind power plant and the source (green) and real power generated by the distribution grid (blue).

The total real power generated by the wind power plant and the source (green) and the real power generated by the distribution grid equivalent (blue) is presented in Figure 61. It can be observed that the total power generated by the wind power plant and the source is 19.72 MW, which is also the real power flowing through the circuit breaker under investigation. The distribution grid equivalent is consuming 19.57 MW of real power, which is lower than the total generated power due to losses in the overhead lines.

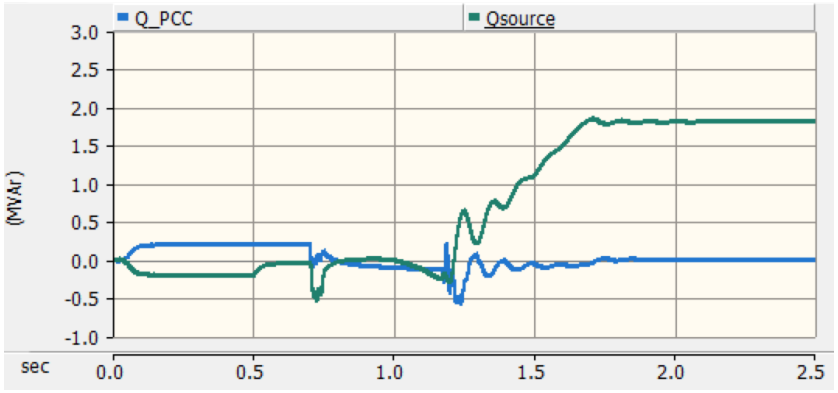

Figure 62: Reactive power generated by one wind turbine (blue) and reactive power generated by the source (green).

The reactive power generated by one wind turbine and by the source is shown in Figure 62. The reactive power generated by one wind turbine is 0 MVar, while the reactive power generated by the source is 1.81 MVar. Both of these values have reached steady state at 2.1 sec.

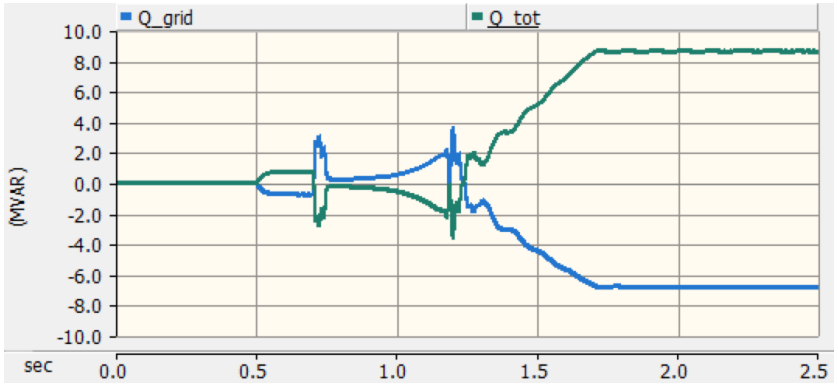

Figure 63: Total reactive power generated by the wind power plant and the source (green) and reactive power generated by the distribution grid equivalent (blue).

In Figure 63 the total reactive power generated by the wind power plant and the source (green) and the reactive power generated by the distribution grid equivalent (blue) is presented. The reactive power generated by the wind power plant and the source is 8.63 MVar, while the reactive power consumed by the distribution grid equivalent is 6.82 MVar. The difference between the generated and consumed reactive power is caused by reactive power consumption in the overhead lines.

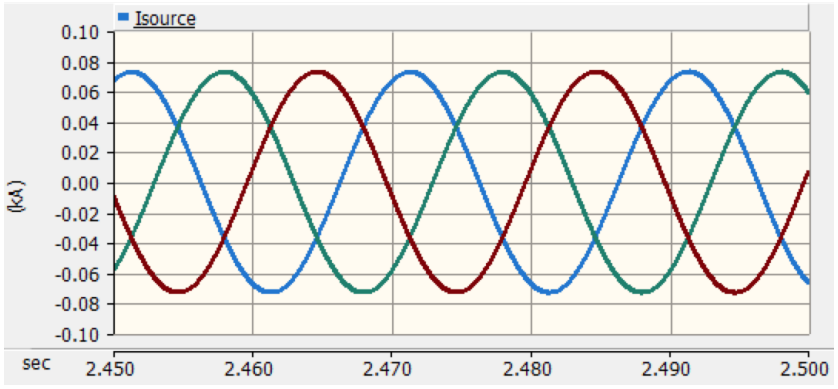

Figure 64: Output current from the source.

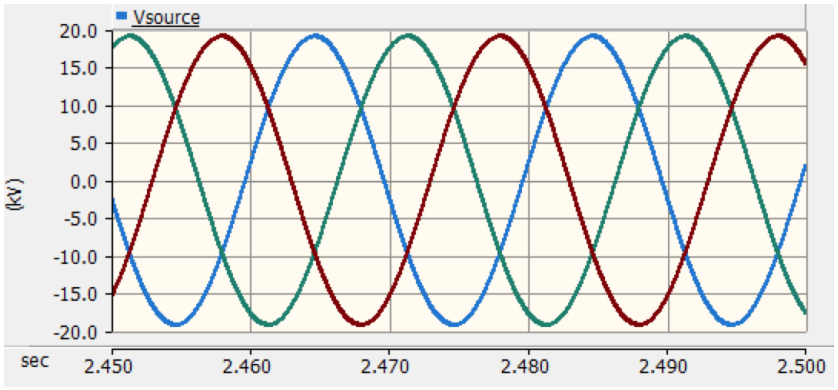

Figure 65: Output voltage from the source.

In Figure 64 and Figure 65 the output current and voltage from the source is shown. The peak value of the voltage is 19.14 kV line to ground, while the peak of the current is 0.07 kA. By comparing the output current from the source to the output current from one wind turbine it can be observed that the output current from one wind turbine is 2.4 times the output current from the source. The output voltage from the source is equal to the output voltage from one wind turbine.

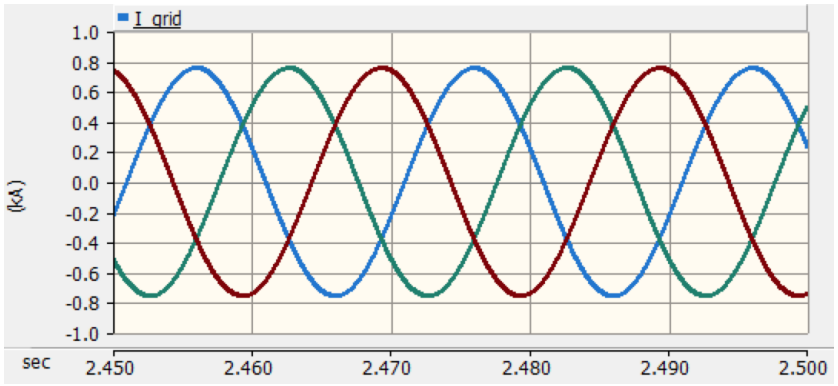

Figure 66: Current flowing into the distribution grid equivalent.

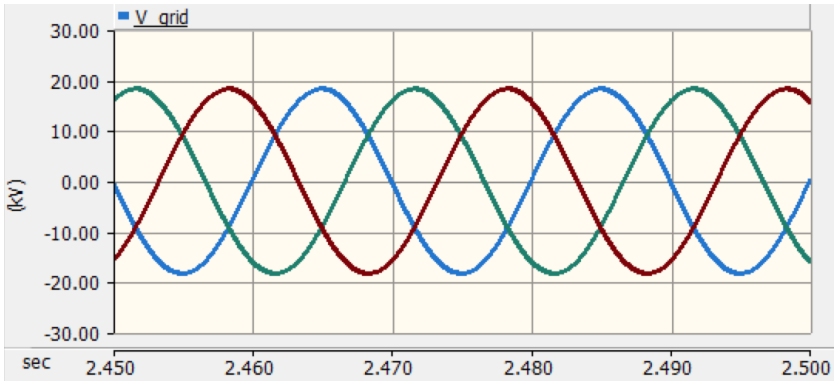

Figure 67: Phase voltage at the terminal of the distribution grid equivalent.

In Figure 66 and Figure 67 the current and phase voltage measured at the terminal of the distribution grid equivalent is shown. The peak value of the current is 0.76 kA. By comparing this current to the current flowing into the distribution grid equivalent in the PV network of 0.81 kA, it can be observed that these two currents are within the same range. The peak value of the phase voltage is 18.28 kV, which corresponds to $18.28 * \frac{\sqrt{3}}{\sqrt{2}} = 22.39$ kV line to line RMS. This line to line RMS voltage is within the 7 % margin.

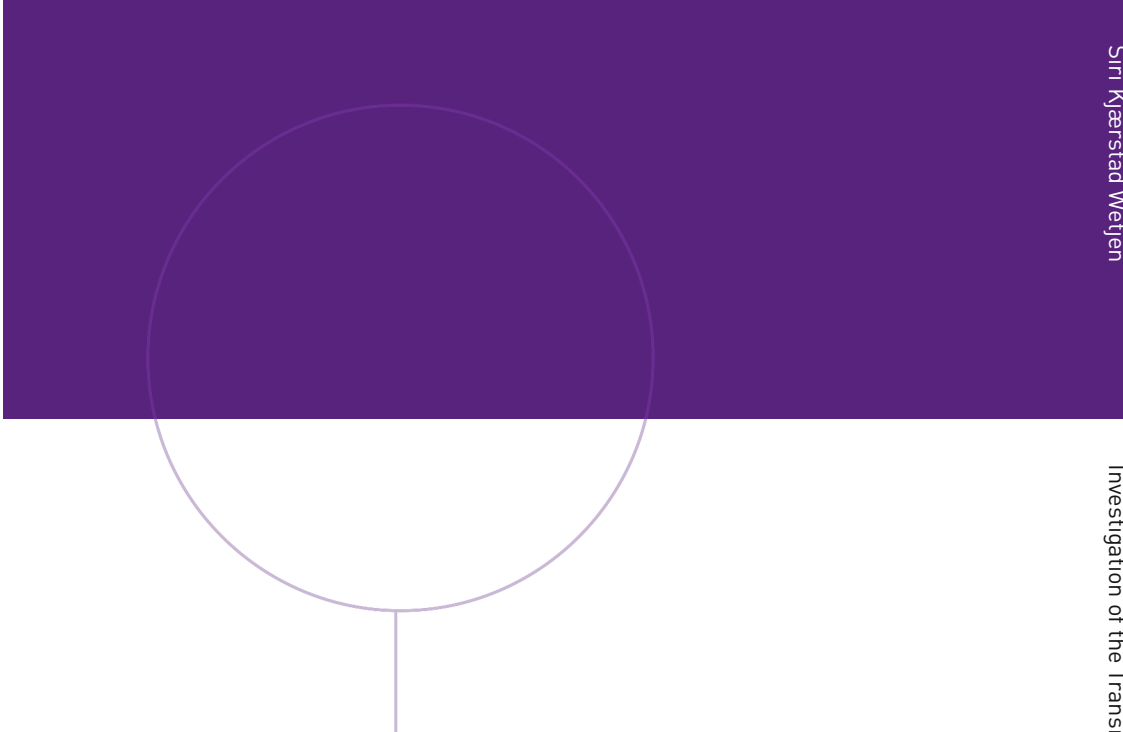

Siri Kjærstad Wetjen

Investigation of the Transient Recovery Voltage across Circuit Breakers in Networks with Distributed Energy Resources

NTNU
Norwegian University of
Science and Technology